Methylsulfonyl and Methoxysulfinyl Radicals and Cations in the Gas Phase. A Variable-Time and Photoexcitation Neutralization−Reionization Mass Spectrometric and ab Initio/RRKM Study

Aaron J. Frank and Frantisek Turecek*

Department of Chemistry, Bagley Hall, Box 351700, University of Washington, Seattle, Washington 98195-1700

Received: March 17, 1999; In Final Form: May 4, 1999

The title radicals were produced by femtosecond collisional electron transfer in the gas phase and studied by the methods of variable-time neutralization−reionization mass spectrometry combined with fast-beam laser photoexcitation and G2(MP2) ab initio/RRKM calculations. The methylsulfonyl radical ($CH_3SO_2^•$, **1)** was calculated to be bound by 59 kJ mol^{-1} against the lowest-energy dissociation to $CH_3^•$ and SO_2 at 0 K and to have a heat of formation $\Delta H_{f,298}(\mathbf{1}) = -211 \pm 4$ kJ mol^{-1}. When formed by vertical electron transfer, radical **1** dissociated rapidly due to a large Franck−Condon energy, $E_{FC} = 141$ kJ mol^{-1}. The reverse addition of $CH_3^•$ to the sulfur atom in SO_2 had a potential energy barrier of 1.3 kJ mol^{-1} and Arrhenius parameters, log $A = 12.19$ and $E_a = 5.4$ kJ mol^{-1}. The calculated addition rate constant, $k_{295} = 1.7 \times 10^{11}$ cm^3 mol^{-1} s^{-1}, was in excellent agreement with the previous measurement of Simons et al. The methoxysulfinyl radical ($CH_3OSO^•$, **2**) was calculated to exist as an equilibrium mixture of syn (**2s**) and anti (**2a**) conformers. The Boltzmann-averaged heat of formation of **2** was calculated as $\Delta H_{f,298}(\mathbf{2}) = -230 \pm 4$ kJ mol^{-1}. Vertical neutralization of ions $\mathbf{2s}^+$ and $\mathbf{2a}^+$ produced substantial fractions of stable **2s**,**a**. Dissociating **2s**,**a** formed $CH_3^•$ and SO_2 through unimolecular isomerization to **1**. Direct dissociation of the C−O bond in **2s**,**a** to form $CH_3^•$ and SO_2 was calculated to have a large activation barrier (152 kJ mol^{-1} from **2a**) and did not compete with the isomerization to **1**, which required 111 kJ mol^{-1} from **2a**. Photoexcitation of **2s**,**a** resulted in a slightly increased formation of $\mathbf{2s,a}^+$. This was interpreted with the help of CIS/6-311+G(3df,2p) calculations as being due to the formation of a bound excited *B* state of **2s** upon electron transfer. The *B* state was photoexcited at 488 and 514.5 nm to high Rydberg states which were predicted to have large cross sections for collisional ionization. The *A* state of **2s** was calculated to be bound but photoinactive. The *C* through *E* states of **2s** were unbound and predicted to dissociate exothermically to CH_3OS and (^{3}P)O.

Introduction

The oxidation cascade reactions converting the so-called reduced sulfur compounds (H_2S, dimethyl sulfide, dimethyl disulfide, etc.) to oxidized sulfur compounds (SO_2, sulfuric acid, and methanesulfonic acid) in the troposphere involve several reaction intermediates.[1−4] The concentrations of these intermediates in the troposphere are very small, which makes direct observation and characterization difficult. Some of the proposed intermediates in the oxidation of dimethyl sulfide and dimethyl disulfide belong to the family of [C, H_3, S, O_2] radical isomers. There have been several computational studies which addressed the structure of [C, H_3, S, O_2] radicals and cations.[5−10] Reactions of $CH_3^•$ and SO_2 to form methylsulfonyl and methoxysulfinyl radicals were previously examined at intermediate levels of theory.[7] The stabilities of the methylsulfonyl and methoxysulfinyl radicals were addressed and the methyloxysulfinyl radical was determined to be the most stable isomer, while the sulfonyl radical was less stable.[6,7] In addition, the methanethiylperoxy radical $CH_3SOO^•$ has received considerable attention in the past few years.[6−8] The weakly bound methanethiylperoxy radical, formed by addition of O_2 to $CH_3S^•$, was investigated theoretically and shown to have varying degrees of stability depending upon the level of theory used.[6−8] Reaction of $CH_2SH^•$ with O_2 was recently examined to model a possible intermediate in the gas-phase reaction of $CH_2SH^•$ with atmospheric gases.[5]

Experimentally, [C, H_3, S, O_2] radicals have been studied by spectroscopy[11−23] and various gas-phase reaction techniques. Additional reactions between $CH_3S^•$ and atmospheric gases such as O_3, NO_2, and NO have been extensively studied along with mechanistic and kinetic descriptions of these reactions.[24−28] One of the products formed from these reactions was $CH_3O^•$, which can react further to produce $CH_3SO_2^•$. The adduct formed between $CH_3S^•$ and O_2 was observed at low temperatures (−57 °C to −15 °C) and was estimated to be bound by ∼11 kJ mol^{-1}.[26] Reactions of sulfinyl and sulfonyl cations were recently studied.[29−32] However, in some of these studies, direct observation of both the parent and its fragments was not feasible, and in many cases it was impossible to create and distinguish different isomers. Therefore, we used neutralization−reionization mass spectrometry (NRMS) along with high-level computational methods to address the stability and reactions of selected [C, H_3, S, O_2] radicals and cations in the gas phase.

NRMS relies on collisional neutralization of fast, stable cations or anions in the gas phase.[33] Owing to an extremely short time for the interaction between the fast ion and the thermal atomic or molecular target ($<10^{-14}$ s),[33c] collisional electron transfer produces the transient fast radical or molecule with the structure and geometry of the ion precursor. Reaction products resulting from unimolecular or collision-induced dissociations of transient neutral species are analyzed by mass spectrometry following collisional reionization. NRMS has been used to

10.1021/jp990946z CCC: $18.00
Published on Web 06/19/1999

generate and study a number of transient, oxygenated sulfur molecules and radicals, e.g. $HSO^{\bullet}$ and $SOH^{\bullet}$;[34] CH_3SOH, CH_2-$SHOH$, $CH_3SO^{\bullet}$, and $CH_2SOH^{\bullet}$;[35] $HSO_3^{\bullet}$;[36] H_2SO_3;[37] $CH_2{=}CH{-}SOH$ and $CH_3CH{=}S{=}O$;[38] $(CH_3)_2SOH^{\bullet}$,[39] $SO_2H^{\bullet}$, $HSO_2^{\bullet}$, and SO_2H_2;[40] HOSSOH;[41] and H_2SO and HSOH,[42] as reviewed recently.[43]

The capabilities of NRMS for studying unimolecular neutral dissociations have been extended recently by the introduction of the variable-time method, which uses different temporal profiles of neutral dissociations and post-reionization ion dissociations to distinguish these processes and also provides the pertinent unimolecular rate parameters.[44] Ground and excited electronic states of the neutral species formed by femtosecond electron transfer can be probed by laser photoionization and photoexcitation.[40,45] We now apply these methods to the preparation and characterization of isomeric methylsulfonyl (**1**) and methoxysulfinyl (**2**) radicals and a deuterium labeled derivative, CD_3SO_2 (**1D**). Since NR mass spectra do not provide direct information about the energetics of transient neutral intermediates, ab initio calculations at an augmented G2(MP2) level of theory are used to provide relative energies and dissociation barriers. The latter are used for RRKM calculations[46] of unimolecular rate constants and transition-state theory calculations of rate constants for bimolecular addition reactions.

Experimental Section

The following experiments were performed on a home-built tandem quadrupole acceleration deceleration mass spectrometer which was described in detail previously.[47] The ions were formed in an electron impact source by dissociative ionization of methyl sulfone and dimethyl sulfite to give $[C, H_3, S, O_2]^+$ ions. Typical conditions were as follows: Electron energy 70 eV, electron current 500 μA, ion energy ~80 eV, and source temperature 230−270 °C. The ions were extracted from the source and passed through a quadrupole operated in the radio-frequency-only mode. A series of lenses accelerated the ions to reach the final translational energy of ca. 8200 eV. The fast ions entered a collision cell in which a neutralization gas was introduced to achieve 70% transmittance (*T*) of the precursor ion current. At this transmittance, >85% of the colliding ions underwent single collisions. The neutralization gases used in these experiments were trimethylamine, di-*n*-butylamine, and xenon. The neutrals and ions exited the collision cell and entered the conduit region. The fast ions were reflected by the first element of the conduit, which was floated at +250 V while the neutrals passed unhindered. The lifetime of the neutrals in the 60-cm-long conduit was 4.2 μs. The surviving neutrals and fragments were then reionized in a second collision cell by O_2 introduced to achieve 70% *T* of the precursor ion current. The fast ions were decelerated to ~80 eV translational energy, energy filtered, mass analyzed by a second quadrupole, and detected by an off-axis electron multiplier. The electron current was converted to a voltage and amplified by a Keithley 428 amplifier. A series of consecutive scans, usually 20−30 per spectrum, were collected and processed by a PC-based control system.

Charge exchange ionization experiments were performed in a tight chemical ionization (CI) source. Ordinarily, Xe was introduced to achieve a pressure of 6×10^{-4} Torr which was measured on a Bayard−Alpert type ionization gauge located on the diffusion pump intake. The pressure inside the chemical ionization source was estimated to be ~0.5 Torr.

Neutralization-collisional activation−reionization (NCR) experiments were performed by introducing a collisional gas into the conduit. Typically, He was introduced to achieve either 70%, 50%, or 30% *T* of the precursor ion current. The products and surviving neutrals were reionized in a manner similar to the standard NRMS method.

Variable time experiments were performed using the procedure described previously.[44] The lifetimes of the neutrals and reionized fragments and survivor ions were varied in an inverse fashion by applying a scanning high voltage potential to various portions of the conduit. Using the ratio of integrated peak intensities for the survivor ion to fragment ion and reionization efficiencies (calculated using the method of Fitch and Sauter[48]), the dissociation rate constants for neutral and ionic dissociations could be calculated. A least-squares fit was calculated for a bimodal exponential decay for one fast and one slow dissociation in the neutral channel and for a single-exponential decay in the ion channel. A Visual Basic macro was used to integrate the kinetic equations for unimolecular dissociations for both neutrals and ions.

Photoexcitation experiments were performed using the method described previously.[45] A Coherent Innova 90 CW argon−ion laser was used so that the laser radiation was shone coaxially through the neutral and ion beam. It was estimated that >40% of the ~3-mm-diameter laser beam overlapped with the neutral and ion beam. A transparent indium tin−oxide (ITO)-coated window was used in the energy filter to allow the laser radiation to pass into the conduit region. The conductive ITO window also prevented charge buildup on this lens. Losses due to the window were less than 9% when the laser was operated at 5.5 W. The light intensity in the neutral drift region was >1.5 W. At this power, the photon flux was in the 10^{19} photons s^{-1} range. The main lines were the 488 and 514.5 nm, which corresponded to 2.54 and 2.41 eV, respectively. The low-intensity short wavelength lines were largely removed by the ITO window, and therefore the neutral beam was not exposed to photon energies greater than 2.54 eV. Oxygen was introduced over the conduit while the electrostatic potential on the conduit elements was scanned in link with the deceleration potentials. In this fashion, the products due to photofragmentation and collisional reionization formed in the high-voltage scanned region of the conduit were detected selectively.

Collision induced dissociation (CID) experiments were performed on a JEOL-HX100 double-focusing mass spectrometer using linked B/E scans. The CID gas used was air, unless noted otherwise.

Materials. Trimethylamine (Matheson 99%), O_2 (Air Products 99%), He (General Welding Supply Co., Seattle, 99.99%), methyl sulfone (Aldrich, 98%), and dimethyl sulfite (Aldrich, 99%) were used as received. The purity of methyl sulfone and dimethyl sulfite was confirmed by GC−MS. Methyl-d_6-sulfone was prepared by oxidizing 2.0 g dimethyl-d_6-sulfoxide (Cambridge Isotope Laboratories, 99% d) in 2 mL acetic acid with a 100% excess of H_2O_2. The H_2O_2 was added dropwise to the sulfoxide solution, and the solution was heated to 70 °C for 2 h. A 20% Na_2CO_3 solution was added, and then the product was extracted into three 50-mL aliquots of $CHCl_3$. The solvent was distilled off, and the solid product was dried in vacuo at 25 °C. The product yield was 64%. Subsequent GC−MS analysis indicated one product with a mass spectrum corresponding to the indicated product.

Calculations. Standard ab initio and density functional theory calculations were performed using the Gaussian 94 suite of programs.[49] Geometries were optimized at two levels of theory. Optimized geometries for $[C, H_3, S, O_2]$ radicals and cations were obtained using Becke's hybrid functional (B3LYP)[50] and

the 6-31+G(2d,p) basis set. The latter is a split-valence basis set furnished with diffuse functions and a split shell of d functions on C, O, and S.[51] Basis sets of this quality have been shown to give mostly reliable equilibrium geometries for radicals and ions.[52] Since geometry optimizations of sulfur radicals can be difficult and may depend on the basis set and method used,[53] the key structures were reoptimized with perturbational Moller−Plesset treatment of correlation energy,[54] MP2(FULL), using the 6-31+G(2d,p) basis set. Spin-unrestricted calculations (UHF and UMP2) were used for radicals. Spin contamination in the UMP2 calculations caused the expected spin values $\langle S^2 \rangle$ to be 0.77−0.79. Projection by spin annihilation[55] reduced the $\langle S^2 \rangle$ values to 0.75−0.77 and resulted in PMP2 total energies that were 2−5 millihartree lower than the UMP2 values. The optimized structures were characterized by harmonic frequency analysis as local minima (all frequencies real) or first-order saddle points (one imaginary frequency). The B3LYP/6-31+G(2d,p) frequencies were scaled by 0.963[56] and used to calculate zero-point energies, enthalpy corrections, and RRKM rate constants. Single-point energies were calculated at the Gaussian-2(MP2) level of theory.[57] This consisted of MP2/6-311+G(3df,2p), MP2/6-311G(d,p), and QCISD(T)/6-311G(d,p)[58] calculations which were combined to provide effective QCISD(*T*)/6-311+G(3df,2p) energies, which were corrected for the ZPVE and the number of valence electrons.[57] Note that most relative energies calculated in this work refer to isoelectronic systems or isogyric reactions in which the empirical corrections cancel out. The G2(MP2) energies were much less sensitive to spin contamination; the use of PMP2 energies resulted in G2(MP2) energies that were <0.9 millihartree (rmsd) lower than those that used UMP2 energies. Excited electronic states in **1** were investigated with Configuration Interaction Singles (CIS)[59] calculations. Geometry optimizations were performed with spin-unrestricted CIS/6-31+G(2d,p) calculations. Single-point energies were calculated with CIS/6-311+G-(3df,2p).

RRKM calculations were performed with using Hase's program,[60] which was recompiled for MS-DOS and run under Windows NT. Vibrational state densities were obtained by direct count of quantum states in 0.4 kJ mol^{-1} steps for internal energies up to 60−100 kJ mol^{-1} above the threshold. The rotational states were treated adiabatically,[61] and the microscopic rate constants, *k(E, J, K)*, were Boltzmann-averaged over the thermal distribution of rotational J and K states pertaining to the ion source temperature (200 °C).

Results

As documented by the experiments and calculations described below, the formation of methoxysulfinyl cations (**2s,a**$^+$) and radicals (**2s,a**) was straightforward, whereas the preparation of the methylsulfonyl cation (**1**$^+$) and radical (**1**) was more involved. The former species are, therefore, discussed first.

Formation of Methoxysulfinyl Cations and Radicals. The precursor cations, a mixture of conformational isomers **2a**$^+$ and **2s**$^+$, vide infra, were formed by dissociative ionization of dimethyl sulfite using 70 eV electrons. The pressure inside the source was estimated to be $<10^{-5}$ Torr, which indicated that the ions were formed by unimolecular dissociations. As shown in Scheme 1, loss of a methoxy radical from the dimethyl sulfite radical−cation gave *m/z* 79, $[C, H_3, S, O_2]^+$, which was the base peak in the mass spectrum. The ions were characterized by collision-induced dissociation (CID) spectra obtained under high mass-resolution conditions using air at 70% *T* as the collision gas (Figure 1). The primary ion dissociation of **2s,a**$^+$ was the loss of OCH_3 to form $SO^{+\bullet}$, which gave 43.0% of the total fragment ion current, while the formations of $SO_2^{+\bullet}$ (by loss of CH_3) and $[S, O, H]^+$ (by loss of CH_2O) were comparable (11%). The ion dissociation to form CH_2OSO^+ was relatively inefficient, 4.3%.

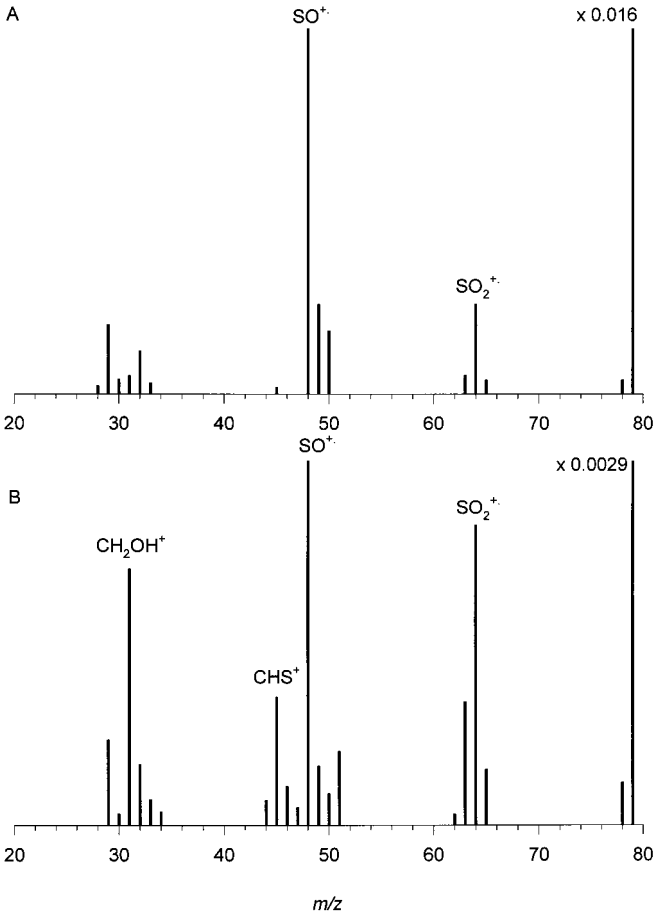

Figure 1. Collision-induced dissociation mass spectra of (A) **2s,a**$^+$ and (B) **1**$^+$. Air was used as collision gas at 70% transmittance of the precursor ion beam.

SCHEME 1

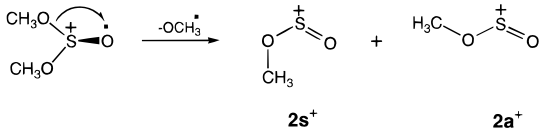

The fast ions were neutralized with a series of gases of increasing vertical ionization energies, trimethylamine (TMA, IE_v = 7.85 eV), di-*n*-butylamine (DBA, IE_v = 8.45 eV), and Xe (IE_v = 12.13 eV). Based on the calculated vertical recombination energy (RE_v) of the precursor cation (**2a**$^+$, RE_v = 7.7 eV; **2s**$^+$, RE_v = 8.1 eV, vide infra), the neutralization processes were ∼0.25 eV exothermic to ∼4.4 eV endothermic. The neutralization−reionization mass spectrum, using TMA as the neutralization gas, of **2s,a**$^+$ indicated a moderate survivor ion, 14% of the sum of the NR ion intensities (ΣI_{NR}, Figure 2), while DBA produced a slightly less intense survivor ion (10% ΣI_{NR}). Using Xe as the neutralization gas, the survivor ion intensity decreased to 5.7% ΣI_{NR}. Primary dissociations observed corresponded to the loss of hydrogen, methyl, and methoxyl, which were only slightly affected by the nature of the neutralization gas.

The internal energy of the intermediate radicals **2s,a** was increased by collisional activation (CA) with He (Figure 3). Helium was introduced over the conduit at a pressure to reduce

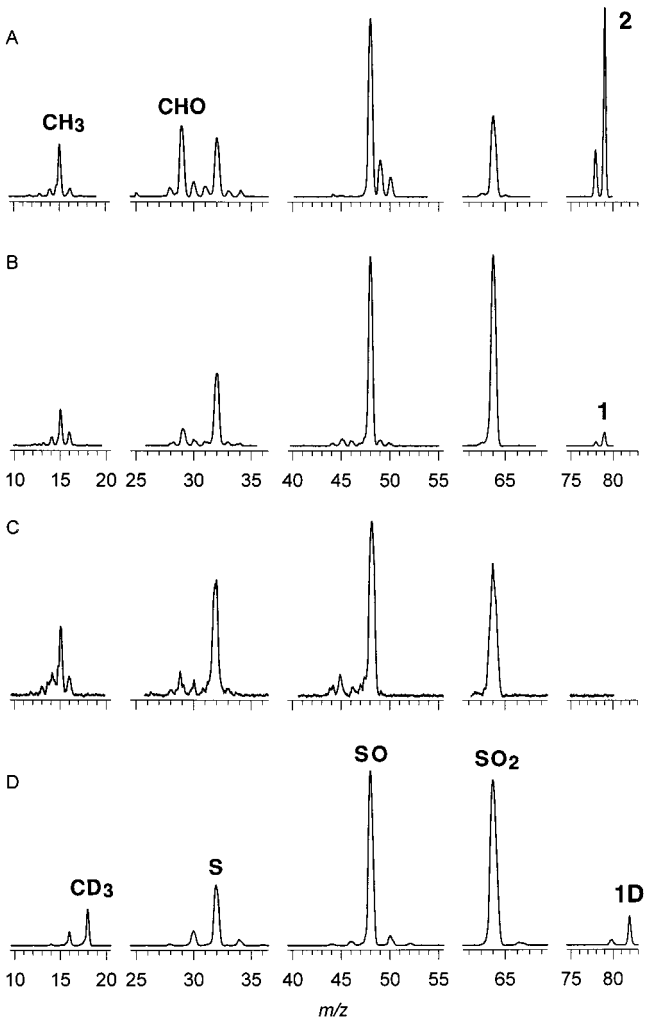

Figure 2. Neutralization (trimethylamine, 70%*T*)−reionization (O_2, 70%*T*) mass spectra of (A) **2s,a**$^+$, (B) **1**$^+$ prepared by 70-eV electron impact ionization of methyl sulfone, (C) **1**$^+$ prepared by Xe charge-exchange ionization, and (D) **1D**$^+$.

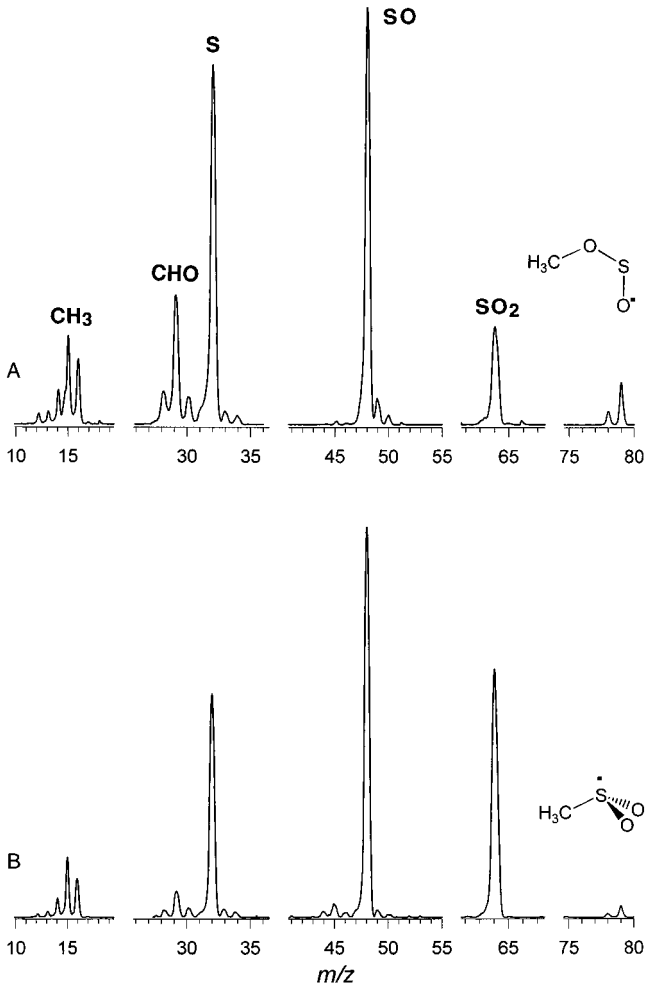

Figure 3. Neutralization (trimethylamine, 70%*T*)−collisional activation (He, 50%*T*)−reionization (O_2, 70%*T*) mass spectra of (A) **2s,a**$^+$ and (B) **1**$^+$.

the precursor ion beam to 70%, 50%, and 30% transmittance (*T*). At 70% *T*, the survivor ion peak decreased to 8.9% ΣI_{NR}, while at 30% *T*, the survivor ion peak was 2.6% ΣI_{NR}. When the probability of multiple collisions was increased, the ratio of relative abundances, $[SO_2^{+\bullet}]/[SO^{+\bullet}]$ ratio decreased sequentially from 0.49 (no CA) to 0.34 (30% *T*). Secondary dissociations leading to the formation of $S^{+\bullet}$ increased to 22% ΣI_{NR} at the lowest transmittance. The $[C,H_3,O^+]$ and the CH_3^+ fragments remained relatively constant 13.4 ± 0.8% ΣI_{NR}, and 5.6 ± 0.3% ΣI_{NR}, respectively.

The neutral and post-reionization ion dissociations were distinguished using variable-time experiments. The relative integrated ion currents for [**2s,a**$^+$], $[CH_3^+]$, $[SO_2^{+\bullet}]$, and $[SO^{+\bullet}]$ were obtained from the time-dependent experiments. The $[CH_3O^+]$ ion intensity was estimated by using the sum of intensities from *m*/*z* 28 through 31, because the methoxy cation is known to dissociate to form these ions.[62] To further identify neutral dissocations, the dissociation rate constants for the formation of complementary products were compared. Correlation of the rate constants for neutral dissociations (k_N) provided an important criterion that the products originate from a single precursor and not by consecutive dissociations.[44c]

Formation of SO_2 and $CH_3^\bullet$ by neutral dissociation followed by reionization was observed in the NR mass spectra of **2s,a**. Likewise, neutral dissociations were observed for the formation of SO and $^\bullet OCH_3$. Correlation of the rate parameters for the complementary products of neutral dissociations was reasonably good for both reactions, $k_N(SO_2) = (3.6 \pm 0.5) \times 10^5\ s^{-1}$ and $k_N(CH_3) = (3.1 \pm 1.6) \times 10^5\ s^{-1}$, while $k_N(SO) = (6.1 \pm 0.8) \times 10^5\ s^{-1}$ and $k_N(OCH_3) = (4.9 \pm 1.3) \times 10^5\ s^{-1}$. The rate constants for ion dissociations were smaller for both reactions: $k_i(SO_2^{+\bullet}) = (2.2 \pm 1.0) \times 10^5\ s^{-1}$, $k_i(CH_3^+) = (0.5 \pm 0.2) \times 10^5\ s^{-1}$, and $k_i(SO^{+\bullet}) = (3.4 \pm 1.8) \times 10^5\ s^{-1}$, $k_i(OCH_3^+) = (1.3 \pm 1.3) \times 10^5\ s^{-1}$. Note that the rate parameters for ion dissociations do not correlate in general due to the difference in the ionization energies for each species. The unimolecular dissociations of **2s,a** to form H + CH_2OSO were also examined. The neutral rate constant was $k_N(CH_2OSO) = (0.7 \pm 0.2) \times 10^5$, while the rate constant for the ion dissociation was $k_I(CH_2OSO^{+\bullet}) = (0.5 \pm 0.5) \times 10^5$. The corresponding dissociation rate constants for the formation of H^+ were not monitored because of the low-mass cutoff of the mass-analyzing quadrupole.

Formation of Methylsulfonyl Cation and Radical. Methylsulfonyl cation, **1**$^+$, was prepared by dissociative ionization of methyl sulfone with 70 eV electrons. The EI mass spectrum of methyl sulfone indicated that *m*/*z* 79, $[C, H_3, S, O_2]^+$ was the base peak. Ion **1**$^+$ was characterized by the CID spectrum, which differed from that of **2s,a**$^+$ (Figure 1B). Major fragment ions were found at *m*/*z* 64 ($SO_2^{+\bullet}$, loss of CH_3, 17.4%), 48 ($SO^{+\bullet}$, 21.1%), 31 (CH_2OH^+, 14.9%), 45 (CHS^+, 7.4%), 63 (CH_3SO^+, 7.1%), and 51 ($[H_3, S, O]^+$, 4.3%). The formation

of $SO^{+\bullet}$, CH_2OH^+, and $[H_3, S, O]^+$ indicated rearrangements in dissociating $\mathbf{1}^+$ and possibly in nondissociating $\mathbf{1}^+$ as discussed below.

Collisional neutralization of stable $\mathbf{1}^+$ was achieved with trimethylamine and Xe. The ΔIE_v for neutralization of $\mathbf{1}^+$ ranged from exothermic for TMA ($\Delta IE_v = -1.76$ eV) to endothermic with Xe ($\Delta IE_v = 2.52$ eV). The NR mass spectrum, obtained by neutralization with TMA, indicated a small survivor ion (1.8% ΣI_{NR}), while the base peak at m/z 64 (SO_2) corresponded to the loss of CH_3, 41% ΣI_{NR} (Figure 2B). A moderately strong peak, 35% ΣI_{NR}, corresponding to SO^+ was also observed, while the loss of H accounted for <1% of the ΣI_{NR}.

This result and the calculated relative stabilities of **1**, $\mathbf{1}^+$, **2s,a**, and $\mathbf{2s,a}^+$ (vide infra) indicated that the survivor ion in the NR mass spectrum of $\mathbf{1}^+$ may be due to a contamination with another stable $[C, H_3, S, O_2]^+$ isomer, most likely $\mathbf{2s,a}^+$. To investigate the effect of precursor ion energy, NR spectra were measured for $\mathbf{1}^+$ produced by CE ionization of methyl sulfone with Xe^+, which was predicted by calculations to yield pure $\mathbf{1}^+$ (vide infra). The NR spectra of thus-prepared $\mathbf{1}^+$ indicated no survivor ion or $(M-H)^+$ peak (Figure 2C). A substantial peak (32% ΣI_{NR}) corresponding to $SO^{+\bullet}$ was observed, while the loss of methyl to produce SO_2 was 20% ΣI_{NR}. It may be noted that subtracting a weighted NR spectrum of $\mathbf{2s,a}^+$ from that of $\mathbf{1}^+$ to annihilate the peak of the survivor ion produced a spectrum that closely resembled the reference NR spectrum of $SO_2^{+\bullet}$, but differed from the NR mass spectrum of the presumably pure $\mathbf{1}^+$ from CE ionization of methyl sulfone. The question of the formation of $\mathbf{1}^+$ and $\mathbf{2s,a}^+$ by EI of methyl sulfone and their contributions to the survivor ion intensity in NR will be further addressed when we discuss the calculated ion and radical energies (vide infra).

Neutralization collisional-activation reionization (NCR) experiments were performed on neutrals from $\mathbf{1}^+$ by introducing He so as to reduce the precursor ion current to 70% and 50% I (Figure 3). At 50% T, the survivor ion was reduced to 0.6% ΣI_{NR}. Likewise, the $SO_2^{+\bullet}$ peak intensity decreased from 34% ΣI_{NR} to 22% ΣI_{NR} in the 50% T NCR experiment, while both the $[SO^{+\bullet}]$ and $[O^{+\bullet}]$ increased to 38% ΣI_{NR} and 3% ΣI_{NR}, respectively, from 34% ΣI_{NR} and 2% ΣI_{NR} in the straight NR experiments. This suggests that **1** dissociated quickly to $CH_3^\bullet$ and SO_2 regardless of further collisonal activation. The SO_2 formed from the fast dissociation of **1** was activated by collisions and dissociated following reionization to eventually give $SO^{+\bullet}$ and $O^{+\bullet}$. Similar effects of collisional activation were observed in the reference NCR spectrum of $SO_2^{+\bullet}$.

Variable-time experiments were performed to elucidate neutral and ion unimolecular dissociations in **1** and $\mathbf{1}^+$. The rate parameters for formation of SO_2 and $CH_3^\bullet$ from neutral dissociations were $k_N(SO_2) = (1.1 \pm 0.2) \times 10^6\ s^{-1}$ and $k_N(CH_3) = (4.9 \pm 1) \times 10^5\ s^{-1}$, respectively, while $k_N(CH_2SO_2) = (9.0 \pm 6) \times 10^4\ s^{-1}$. The rate constants for ion dissociations were $k_I(SO_2^{+\bullet}) = (7.3 \pm 2.6) \times 10^5\ s^{-1}$, $k_I(CH_3^+) = (1.4 \pm 1.2) \times 10^5\ s^{-1}$, and $k_I(CH_2SO_2^{+\bullet}) = (6 \pm 6) \times 10^4\ s^{-1}$. When we included in the kinetic equations an up to 90% fraction of very fast ($k > 10^7\ s^{-1}$) neutral dissociations for the formation of SO_2 and $CH_3^\bullet$, the least-squares fit for the experimental and calculated ion currents improved. This indicated but did not mandate that a large fraction of **1** dissociated within 10^{-7} s. The rather poor correlation between the rate parameters for the formation of neutral SO_2 and $CH_3^\bullet$ from **1** may be due to contamination by **2s,a**, which dissociated to form identical products but with different rate constants (vide supra).

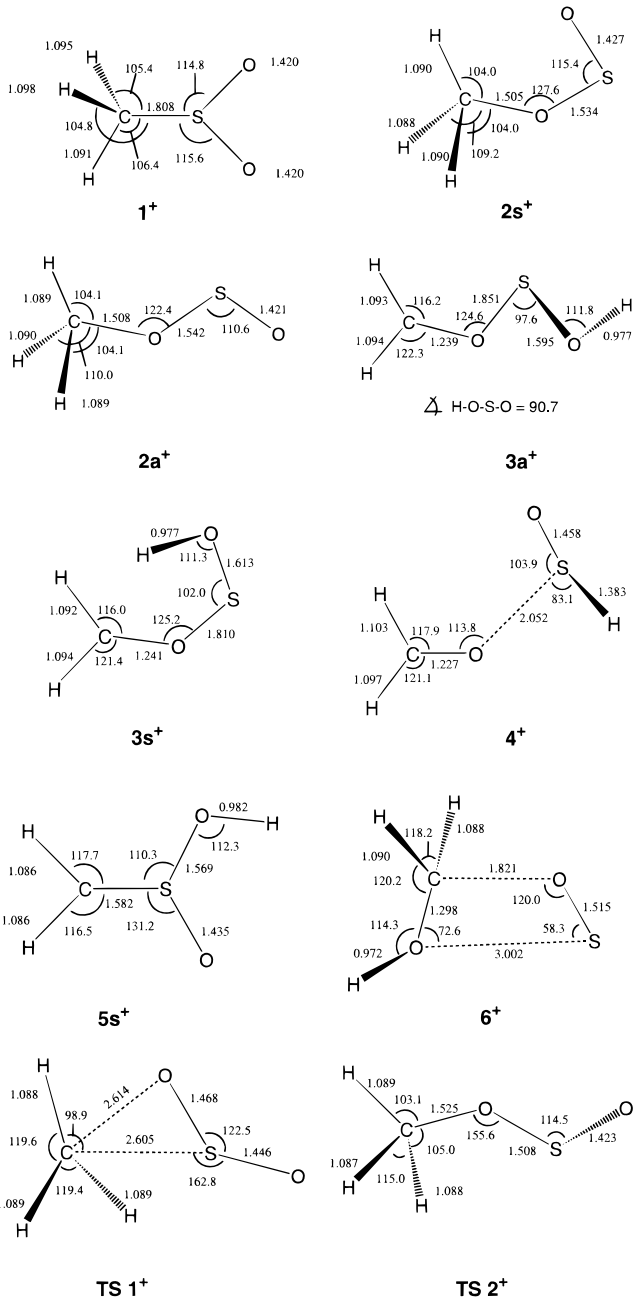

Figure 4. Optimized structures of $[C, H_3, S, O_2]^+$ ions and ion transition states. Bond lengths in Angstroms, bond angles in degrees.

Deuterium labeled ion $\mathbf{1D}^+$ was prepared by dissociative ionization of methyl-d_6-sulfone. Neutralization of $\mathbf{1D}^+$ with TMA resulted in a NR mass spectrum with a slightly larger survivor ion (<3.2% ΣI_{NR}) than that obtained from $\mathbf{1}^+$ (Figure 2D). The loss of CD_3 gave rise to 34% ΣI_{NR}, while the formation of SO increased slightly, 36% ΣI_{NR}. NCR experiments were also performed. The survivor ion current decreased from 2.5% ΣI_{NR} at 70% T with He in the conduit to 0.3% ΣI_{NR} at 30% T. Likewise, the SO_2 peak decreased from 28% to 17% ΣI_{NR} while the peaks corresponding to SO and S increased from 37% to 41% ΣI_{NR} and 16% to 27% ΣI_{NR}, respectively. The variable time experiments indicated neutral dissociation rate constants of $k_N(SO_2) = (7.1 \pm 0.8) \times 10^5\ s^{-1}$ and $k_N(CD_3) = (6.5 \pm 0.2) \times 10^5\ s^{-1}$, which showed a better correlation than those for $\mathbf{1}^+$. The ion dissociation rate constants were $k_i(SO_2) = (2.4 \pm 2) \times 10^6\ s^{-1}$ and $k_i(CD_3) = (9.6 \pm 2) \times 10^5\ s^{-1}$.

TABLE 1: G2(PMP2) Relative Energies of [C, H_3, S, O_2]$^+$ Cations, Radicals, Transition States, and Dissociation Products

Ion	ΔH_0[a]	ΔH_{298}[b]	radical	ΔH_0	ΔH_{298}
			Isomers[d]		
1$^+$	71	71	**1**	21(18)[c]	20
2a$^+$	17	18	**2a**	8(7)[c]	8
2s$^+$	0	0	**2s**	0	0
3a$^+$	71	72	**3a**	166	167
3s$^+$	66	65	**3s**	168	169
4$^+$	85	85	**4**	62	67
5$^+$	135	135	**5a**	134	135
6$^+$	145	145	**5s**	124	125
			Transition States[e]		
TS1(1$^+$ → **2a**$^+$)	136		**TS3(1 → CH$_3$ + SO$_2$)**	60[c]	
TS2(2s$^+$ → **2a**$^+$)	44		**TS4(1 → 2a)**	98	
			TS5(2a → CH$_3$ + SO$_2$)	152	
			TS6(2a → 2s)	1	
			TS7(1 → 1)	239	
			Dissociation Products[d]		
$CH_2OH^+ + (^3\Sigma^-)SO$	155	157	$CH_2 = O + HSO^\bullet$	78	82
$CH_3^+ + SO_2$	235	240	$CH_3^\bullet + SO_2$	80(78)[c]	84
$SO^{+\bullet} + CH_3O^\bullet$	453	456	$CH_2 = O + SOH^\bullet$	100	104
$CH_3^\bullet + SO_2^{+\bullet}$	482	487	$CH_3O^\bullet + (^3\Sigma^-)SO$	257	260
$CH_3OS^+ + (^3P)O$	595	598	$CH_3S^\bullet + (^3\Sigma_u)O_2$	351	354
			syn-$CH_2OSO + H^\bullet$	360	364
			$CH_3OS^\bullet + (^3P)O$	483	487

[a] At 0 K. [b] At 298 K in kJ mol^{-1}. [c] Energies based on MP2(FULL)/6-31+G(2d,p) optimized geometries. [d] Isomer and product energies relative to the most stable ion or neutral species. [e] Transition state energies relative to the reactants.

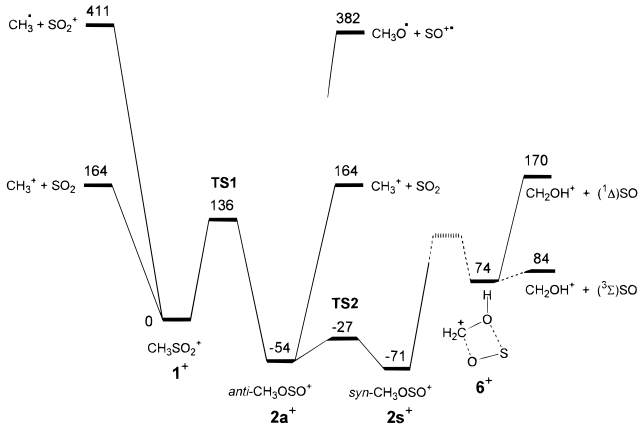

Figure 5. G2(PMP2) potential energy diagram for isomerizations and dissociations of **1**$^+$, **2s**$^+$, and **2a**$^+$ at 0 K in kJ mol^{-1}.

Ion Energetics. To assess the relative stabilities and dissociation energies of the cations used as precursors for the radicals of interest, we obtained optimized geometries and single-point energies for $CH_3SO_2^+$ (**1**$^+$), *syn*-CH_3OSO^+ (**2s**$^+$), *anti*-CH_3OSO^+ (**2a**$^+$), and several other isomers with the $CH_2-O-S-OH$ (**3s**$^+$, **3a**$^+$), $CH_2-O-S(H)=O$ (**4**$^+$), $CH_2-S(=O)-OH$ (**5s**$^+$) and $CH_2-O(H)-S-O$ (**6**$^+$) bond connectivities (Figure 4). The G2(MP2) calculated ion relative enthalpies at 0 and 298 K are summarized in Table 1. Ion **2s**$^+$ was the most stable isomer, followed by **2a**$^+$, **3s**$^+$, **1**$^+$, **3a**$^+$, and **5**$^+$. Ion **4**$^+$ was obtained as an ion−dipole complex of HSO^+ with formaldehyde (Figure 4). Since **1**$^+$ was substantially less stable than **2s**$^+$ or **2a**$^+$, a transition state for unimolecular isomerization of **1**$^+$ to **2a**$^+$ (**TS1**) was also obtained (Figure 4), which had $E_{TS1} = 136$ kJ mol^{-1} above **1**$^+$ (Figure 5). Dissociation of the C−S bond in **1**$^+$ to give CH_3^+ and SO_2 was investigated by B3LYP/6-31+G(2d,p) calculations. The potential energy surface along the dissociation coordinate was continuously endothermic up to the largest separation studied, d(C−S) = 3.7 Å, and did not indicate the presence of an activation barrier. The G2(MP2) dissociation energies of **1**$^+$ were 164 and 168 kJ mol^{-1} at 0 and 298 K, respectively. The 0 K value was 28 kJ mol^{-1} *above* the isomerization barrier to the more stable **2a**$^+$. Hence, a fraction of nondissociating **1**$^+$ could rearrange to **2a**$^+$. The rotational barrier between **2a**$^+$ and **2s**$^+$ (**TS2**) was obtained by G2(MP2) as $E_{TS2} = 44$ kJ mol^{-1} above **2s**$^+$ (Table 1). This showed that **2a**$^+$ and **2s**$^+$ could rapidly equilibrate at energies required for isomerization to **1**$^+$ or dissociation to CH_3^+ and SO_2. The potential energy diagram for the isomerizations and dissociations in **1**$^+$ and **2s,a**$^+$ is shown in Figure 5.

It should be noted that the CID spectra of both **1**$^+$ and **2s,a**$^+$ showed abundant formations of $SO^{+\bullet} + CH_3O^\bullet$ and $[C, H_3, O]^+$. The former dissociation was calculated to require 382 kJ mol^{-1} from **1**$^+$ at the thermochemical threshold, which was much higher than the energy needed for the formation of CH_3^+ and SO_2. Since the latter dissociation did not have an appreciable reverse activation barrier (vide supra), the competitive formation of $SO^{+\bullet}$ indicated that the dissociations occurred from different electronic states in both **1**$^+$ and **2s,a**$^+$.

The lowest-threshold energy was calculated for the formation of CH_2OH^+ and $(^3\Sigma^-)SO$, $\Delta H_{r,0} = 84$ and 155 kJ mol^{-1} from **1**$^+$ and **2s**$^+$, respectively, and was below the threshold for the formation of CH_3^+ and SO_2 (Figure 5). However, the formation of $(^3\Sigma^-)SO$ from singlet **1**$^+$ and **2s,a**$^+$ was spin-forbidden. The threshold for the spin-allowed formation of CH_2OH^+ and $(^1\Delta)SO$ was substantially higher (170 kJ mol^{-1} from **1**$^+$, Figure 5). The formation of CH_2OH^+ required hydrogen migration rearrangements in **2s,a**$^+$. Attempts at optimization of the potential intermediate, $CH_2-O(H)-S-O^+$, resulted in an ion−dipole complex **6**$^+$, which was 145 kJ mol^{-1} less stable than **2s**$^+$. While structure **6**$^+$ may represent an intermediate in the dissociation of **2s,a**$^+$, its high relative energy should prevent it from coexisting with *nondissociating* **2s,a**$^+$ at equilibrium.

The reversible isomerization of **1**$^+$ to **2a**$^+$ was further studied by calculating RRKM rate constants for reaction **1**$^+$ → **2a**$^+$ (k_1) and its reverse (k_{-1}). The calculations yielded log $k_1 = 9.07$ and log $k_{-1} = 8.29$ at the energy corresponding to the threshold of dissociation to CH_3^+ and SO_2. Hence, a fraction of nondissociating ions **1**$^+$ and **2a**$^+$ could isomerize on a time scale which was shorter than the lifetime of the ions sampled for collisional neutralization (10^{-4} s). The equilibrium constant for ion isomerization, $K_{eq} = k_1/k_{-1}$, ranged from 6.5 at the threshold of isomerization to 6.0 at the threshold of dissociation. Since ions **2a**$^+$ and **2s**$^+$, having internal energies close to or greater than the isomerization threshold (190 kJ mol^{-1} for **2a**$^+$), can

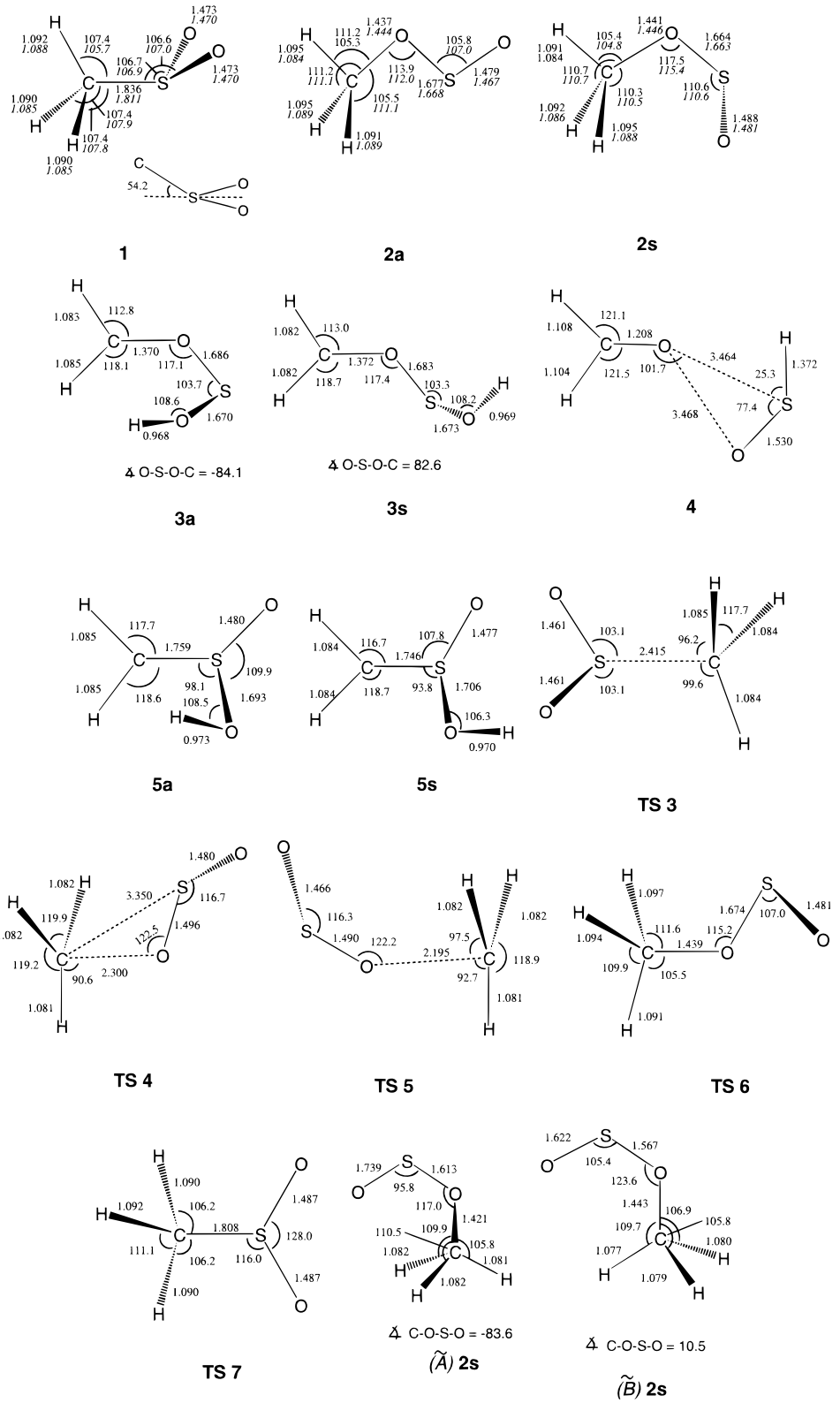

Figure 6. Optimized structures of [C, H_3, S, O_2] radicals and radical transition states. Bond lengths in Angstroms, bond angles in degrees.

rapidly interconvert by internal rotation, the fraction of $\mathbf{1}^+$ within the energy interval between the isomerization barrier and the dissociation threshold can be calculated from a steady-state eq 1, where $\alpha = [\mathbf{2s}^+]/[\mathbf{2a}^+] = 1.44$ and $[\mathbf{1}^+]$, $[\mathbf{2s}^+]$, and $[\mathbf{2a}^+]$ denote the ion fractions. The value of α was calculated from the corresponding partition functions for $\mathbf{2s}^+$ and $\mathbf{2a}^+$. Within the above internal energy limits, the equilibrium fraction of $[\mathbf{1}^+]$

$$[\mathbf{1}^+] = 1/[1 + (\alpha + 1)K_{eq}] \quad (1)$$

was 5.9−6.4%. This, and the fact that a substantial fraction of $\mathbf{2a}^+$ with internal energies <190 kJ mol^{-1} could not isomerize to $\mathbf{1}^+$, implied that nondissociating $\mathbf{2a}^+$ and $\mathbf{2s}^+$ can be prepared as >94% pure mixture of conformers. By contrast, $\mathbf{1}^+$ can be prepared pure only if its internal energy does not exceed the isomerization barrier to $\mathbf{2a}^+$. Tunneling of the CH_3 group

through the isomerization barrier[63] was neglected in these considerations. Note that isomerizations of $\mathbf{1}^+$ to form the other comparably stable ion isomers $\mathbf{3s}^+$, $\mathbf{3a}^+$, and $\mathbf{4}^+$ should require *both* methyl and hydrogen migrations and may involve high-energy intermediates such as $\mathbf{5s}^+$ or $\mathbf{6}^+$ (Table 1). For example, analogous hydrogen migrations from CH_3 to S and from CH_3 to O in protonated dimethyl sulfoxide required 313 and 256 kJ mol^{-1}, respectively.[52b] Thus, rearrangements of $\mathbf{1}^+$ to form the other nondissociating ion isomers were unlikely to be kinetically competitive with the isomerization to $\mathbf{2a}^+$.

To estimate the energy limits for the formation and existence of *stable and nonisomerizing* $CH_3SO_2^+$ ions, we calculated the ion enthalpy of formation, $\Delta H_{f,298}(\mathbf{1}^+)$. The latter was based on the calculated enthalpies for dissociation to CH_3^+ and SO_2 (eq 2), dissociation to CH_3 and $SO_2^{+\bullet}$ (eq 3), and an isodesmic reaction (eq 4) for which there are reliable experimental thermochemical data.[64]

$$CH_3SO_2^+ \rightarrow CH_3^+ + SO_2 \qquad \Delta H_{r,298} = 168.7 \text{ kJ mol}^{-1} \quad (2)$$

$$CH_3SO_2^+ \rightarrow CH_3 + SO_2^{+\bullet} \qquad \Delta H_{r,298} = 416 \text{ kJ mol}^{-1} \quad (3)$$

$$CH_3SO_2^+ + H_2S \rightarrow CH_3SH_2^+ + SO_2 \qquad \Delta H_{r,298} = -172.8 \text{ kJ mol}^{-1} \quad (4)$$

Equations (2)−(4) provided the $\Delta H_{f,298}$ ($\mathbf{1}^+$) as 629.5, 631.2, and 630.4 kJ mol^{-1}, respectively. The average value (630 ± 1 kJ mol^{-1})[65] and the experimental $\Delta H_{f,298}(CH_3) = 146$ kJ mol^{-1} and $\Delta H_{f,298}(CH_3SO_2CH_3) = -373$ kJ mol^{-1} [64] allowed us to estimate the appearance energy (AE) of $\mathbf{1}^+$ from methyl sulfone as 11.91 eV. The upper energy limit for the formation of nonisomerizing $\mathbf{1}^+$ was given by $E_{max} = AE + E_{TS} = 13.32$ eV. These calculations led to the prediction that charge exchange with xenon (IE = 12.13 and 13.44 eV, for the $^2P_{3/2}$ and $^2P_{1/2}$ states, respectively)[66] should result in dissociative ionization of methyl sulfone to produce mostly stable, nonisomerizing $\mathbf{1}^+$. This prediction was actually used to choose the reactant gas in the charge-exchange experiment (vide supra). Note also that ions $\mathbf{1}^+$ formed by the more exothermic charge-exchange ionization with ($^2P_{1/2}$) Xe^+ were cooled by collisions with Xe, which was present in large excess in the ion source.

Radical Structures and Energetics. Optimized geometries were obtained for radicals **1**, **2s**, **2a**, **3s**, **3a**, **4**, **5s**, and **5a** and the transition states for dissociation of **1** to CH_3 and SO_2 (**TS3**), isomerization of **1** to **2a** (**TS4**), dissociation of **2a** to CH_3 and SO_2 (**TS5**), internal rotation in **2a** (**TS6**), and umbrella flipping in **1** (**TS7**) (Figure 6). The radical relative energies are summarized in Table 1. The B3LYP/6-31+G(2d,p) and MP2-(FULL)/6-31+G(2d,p) structures of **1** had staggered C−H and S−O bonds and were similar to that obtained by Davis,[7] but differed from the UHF/6-31G(d) geometry of McKee, which apparently had two eclipsed H−C and S−O bonds.[8] Attempted geometry optimizations of an eclipsed structure resulted in a rotation about the C−S bond to form structure **1**. We note that the eclipsed structure was a saddle point by MP2/6-311G(d,p) geometry optimizations,[7] and its existence as a local minimum was not supported by our calculations. The data further showed the methoxysulfinyl rotamers **2s** and **2a** to be the most stable isomers followed by **1**. The other valence-bond isomers were substantially destabilized against **1** and **2s,a**. Radical **4** dissociated upon attempted geometry optimization to a loose complex of $CH_2{=}O$ and $HSO^\bullet$, which was bound against further dissociation to the components by 16 kJ mol^{-1} at 0 K (Table 1). Interestingly, **3s** and **3a**, which could be viewed as adducts of $CH_2{=}O$ with $SOH^\bullet$, were bound structures which were metastable with respect to exothermic dissociation to $CH_2{=}O$ and $SOH^\bullet$ (Table 1). Hence, the latter dissociation must overcome an activation barrier.

It should be noted that the augmented G2(MP2) calculations provided the correct ordering of relative energies for $HSO^\bullet$ and $SOH^\bullet$, making the former isomer more stable by 22 kJ mol^{-1} at 0 K. This agreed with the previous high-level calculations of Xantheas and Dunning,[53a] according to which $HSO^\bullet$ was 22.6 kJ mol^{-1} more stable than $SOH^\bullet$. Radicals **5s** and **5a** also were high-energy species relative to **2s** (Table 1). Nevertheless, dissociation by O−H bond cleavage in **5s** required 175 kJ mol^{-1} at 0 K, which should have made **5s** amenable to preparation and characterization.

The calculated relative energies for **1**, **2s**, and **2a** were compared with those from previous calculations of Davis, which were based on MP4(SDTQ)/6-311G(d,p) single-point energies.[7] In general, the G2(MP2) 0 K enthalpies (Table 1) showed a greater stability for **1** relative to **2s** and a higher dissociation energy to $CH_3^\bullet$ and SO_2 than was reported by Davis. The 0 K dissociation energy of **2s** to $CH_3^\bullet$ and SO_2 (80 kJ mol^{-1}) was comparable to that calculated by Davis (85 kJ mol^{-1}).[7] The largest qualitative difference was the finding by our calculations of a local minimum for the anti-rotamer **2a**; the latter was found to be a transition state by the previous MP2/6-31G(d,p) calculations.[7] Radical **2a** was separated from the more stable **2s** by a very small rotational barrier, E(**TS6**) = 1 kJ mol^{-1}. Since occasional problems could occur when using DFT methods for location of local minima and transition states in radical additions and dissociations,[67] we reexamined the stationary points for **1**, **2a**, and **2s** with UMP2(FULL)/6-31+G(2d,p) optimizations. The MP2 optimized structures were very similar to those obtained with B3LYP (Figure 6). Consequently, the G2(MP2) single-point energies based on the MP2(FULL) and B3LYP optimized geometries and using the same set of ZPVE corrections were within 1 millihartree (2.6 kJ mol^{-1}). It is likely that the previous failure to locate the local potential energy minimum for **2a** was due to an insufficient basis set for structure optimization. A similar situation has recently been found for the rotamers of the homologous $HO-SO^\bullet$ radical.[40b]

The G2(MP2) energies allowed us to evaluate the standard heats of formation for the stable radicals **1** and **2**. The heat of atomization (eq 5), dissociation (eq 6), and three isodesmic reactions for methyl transfer to (^{3}P)S, $HS^\bullet$, and $CH_3S^\bullet$ (eqs 7−9) were combined with tabulated[64] standard heats of formation to give $\Delta H_{f,298}(\mathbf{1})$ = −213.8, −215.7, −209.9, −206.7, and −209.2 kJ mol^{-1}, respectively. The mean value, $\Delta H_{f,298}(\mathbf{1}) = -211 \pm 4$ kJ mol^{-1}, represents the best estimate at the present level of theory.

$$CH_3SO_2^\bullet \rightarrow (^3P)C + 3(^2S)H + (^3P)S + (^3P)O \qquad \Delta H_{r,298} = 2360 \text{ kJ mol}^{-1} \quad (5)$$

$$\mathbf{1} \rightarrow CH_3^\bullet + SO_2 \qquad \Delta H_{r,298} = 64.7 \text{ kJ mol}^{-1} \quad (6)$$

$$\mathbf{1} + (^3P)S \rightarrow CH_3S^\bullet + SO_2 \qquad \Delta H_{r,298} = -241.1 \text{ kJ mol}^{-1} \quad (7)$$

$$\mathbf{1} + HS^\bullet \rightarrow CH_3SH + SO_2 \qquad \Delta H_{r,298} = -252.3 \text{ kJ mol}^{-1} \quad (8)$$

$$\mathbf{1} + CH_3S^\bullet \rightarrow CH_3SCH_3 + SO_2 \qquad \Delta H_{r,298} = -248.1 \text{ kJ mol}^{-1} \quad (9)$$

To evaluate the $\Delta H_{f,298}$(**2**), reaction enthalpies were calculated for **2s** and **2a** according to dissociations analogous to those in eqs 5, 6, and isodesmic reactions (eqs 10, 11) for methyl transfer to (^{3}P)O, and $OH^\bullet$ to provide the mean heats of formation of

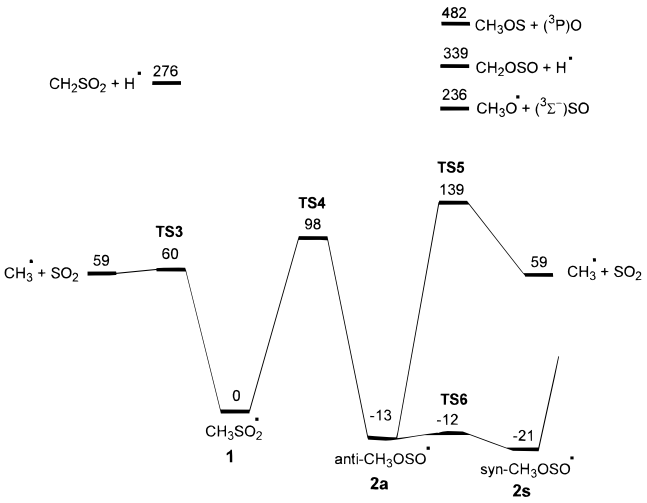

Figure 7. G2(PMP2) potential energy diagram for isomerizations and dissociations of **1**, **2s**, and **2a** at 0 K in kJ mol^{-1}.

the rotamers, $\Delta H_{f,298}(\mathbf{2s}) = -231 \pm 4$

$$syn\text{-}CH_3OSO^\bullet + OH^\bullet \rightarrow CH_3OH + SO_2 \qquad \Delta H_{r,298} = -311.4 \text{ kJ mol}^{-1} \quad (10)$$

$$syn\text{-}CH_3OSO^\bullet + (^3P)O \rightarrow CH_3O^\bullet + SO_2 \qquad \Delta H_{r,298} = -299 \text{ kJ mol}^{-1} \quad (11)$$

kJ mol^{-1} and $\Delta H_{f,298}(\mathbf{2a}) = -223 \pm 4$ kJ mol^{-1}. The latter were Boltzmann-averaged over the rotamer populations at 298 K, which were calculated as 92% **2s** and 8% **2a** from the G2-(MP2) calculated $\Delta G_{298}(\mathbf{2s} \rightarrow \mathbf{2a}) = 6.2$ kJ mol^{-1}. The rotamer-averaged heat of formation was $\Delta H_{f,298}(\mathbf{2}) = -230 \pm 4$ kJ mol^{-1}.

Of particular interest to the present study were the dissociation energies of **1** and **2s**/**2a** (Figure 7). The former radical was only weakly bound with respect to dissociation to $CH_3^\bullet$ and SO_2, $\Delta H_r = 59$ and 64 kJ mol^{-1} at 0 and 298 K, respectively. Dissociation of one of the C−H bonds in **1** to give CH_2SO_2 and H$^\bullet$ was more endothermic and required 276 kJ mol^{-1} at 0 K. The reaction path along the dissociation of the C−S bond in **1** was investigated by B3LYP/6-31+G(2d,p) calculations, which showed continuously increasing potential energy up to the largest separation studied, d(C−S) = 3.5 Å. This differed from the previous calculations of Davis, which showed an early transition state at d(C−S) = 2.36 Å.[7] The potential energy profile along the C−S bond cleavage was therefore reexamined with UMP2(FULL)/6-31+G(2d,p) calculations. These yielded a first-order saddle point, d(C−S) = 2.415 Å. The G2(MP2) single-point energy with ZPVE correction placed the transition state at $E_{TS3} = 60.1$ kJ mol^{-1} above **1**, which was 1.3 kJ mol^{-1} above the products, $CH_3^\bullet + SO_2$ (Table 1). The low TS for the addition was due to a decrease of the TS energy in MP2 calculations when the basis set was expanded from 6-311G-(d,p) to 6-311+G(3df,2p), which resulted in a negative correction to the QCISD(T)/6-311G(d,p) energy. Importantly, the dissociation energy for the reaction **1** → $CH_3^\bullet + SO_2$ (eq 6) was *lower* than the barrier for unimolecular isomerization to **2a**, $E_{TS4} = 98$ kJ mol^{-1} above **1**. This result was consistent with the recent study of S→O-methyl migration in a methylsulfoxide.[68]

Cleavage of the C−O bond to form $CH_3^\bullet$ and SO_2 also was the lowest energy dissociation of **2s** and **2a**; the former rotamer

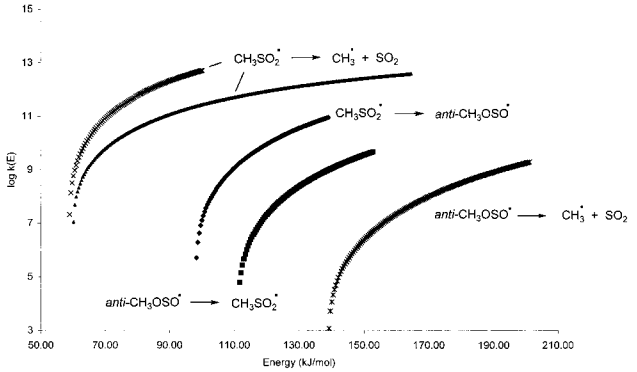

Figure 8. Calculated RRKM rate constants for dissociations and isomerizations in **1** and **2a**. The internal energy scale is relative to **1** for all dissociations.

required 80 and 84 kJ mol^{-1} at 0 and 298 K, respectively. Investigation of the potential energy surface along the C−O dissociation coordinate in **2a** was performed with both B3LYP and UMP2(FULL)/6-31+G(2d,p) calculations. In both cases, the methods yielded a first-order saddle point. That from B3LYP calculations was at d(C−O) = 2.195 Å (Figure 6). The G2-(MP2) potential energy barrier was at $E_{TS5} = 152$ kJ mol^{-1} relative to **2a**, which was 80 kJ mol^{-1} *above* the dissociation threshold to $CH_3^\bullet$ and SO_2 (Figure 7). Previous calculations by Davis predicted an 83 kJ mol^{-1} barrier for the $CH_3^\bullet$ addition to the oxygen atom in SO_2 to form **2s**.[7] Hence, the existence of a potential barrier implied that dissociating **2a** (or **2s**) could competitively isomerize to hot **1**, which will decompose rapidly by C−S bonds cleavage to yield $CH_3^\bullet$ and SO_2.

The other dissociations of **2s** and **2a** were substantially more endothermic. Cleavage of the S−O bond in **2s** to give $CH_3O^\bullet$ and $(^3\Sigma^-)$SO required 257 kJ mol^{-1} at 0 K. Cleavage of a C−H bond in **2s** to form CH_2O−SO and H$^\bullet$ was even more endothermic and required 360 kJ mol^{-1} at the thermochemical threshold at 0 K (Table 1). The potential energy barriers along the latter two high-energy dissociation pathways were not investigated.

Dissociation Kinetics. The kinetics of competing unimolecular isomerization of **1** to **2a** and dissociations to $CH_3^\bullet$ and SO_2 were investigated by RRKM calculations (Figure 8). With **1**, the calculations were performed for both the transition state, located by UMP2(FULL) optimizations, and the barrierless dissociation, predicted by B3LYP optimizations. For the latter, unimolecular rate constants were calculated using variational transition state theory (VTST).[69] The *k(E)* calculated by VTST for d(C−S) = 2.8 Å were consistently greater than those obtained for dissociations involving the potential energy barrier. However, regardless of the potential energy surface used, the dissociation of **1** was more than an order of magnitude *faster* than the isomerization to **2a** at all relevant internal energies (Figure 8). Therefore, it can be safely stated that **1** could not isomerize unimolecularly to the more stable **2a** and hence to **2s**. In contrast, dissociation of **2a**, which had a substantial energy barrier (Figure 7), was 2−3 orders of magnitude *slower* than unimolecular isomerization to **1** (Figure 8). This indicated that the dissociation of **2a** or **2s** to $CH_3^\bullet$ and SO_2 proceeded through **1** as a transient intermediate.

The calculated activation barriers for addition of $CH_3^\bullet$ to the sulfur atom in SO_2 and the reverse dissociation of **1** ($E_a = 60.1$ kJ mol^{-1}) were further used for transition-state theory calculations[70] of the corresponding rate constants, k_{add} (eq 12) and k_{dis} (eq 13), at the high pressure

$$k_{add} = \frac{k_B T V_M N_A}{h} \frac{Q(\mathbf{TS})}{Q(\mathbf{SO_2})Q(\mathbf{CH_3})} e^{-E_0/k_B T} \quad (12)$$

$$k_{dis} = \frac{k_B T}{h} \frac{Q(\mathbf{TS})}{Q(\mathbf{1})} e^{-E_0/k_B T} \quad (13)$$

limit, where k_B is the Boltzmann constant, V_M is the molar volume, N_A is the Avogadro number, h is the Planck constant, E_0 is the G2(MP2) energy barrier, and the partition functions, $Q = Q_{el}Q_{trans}Q_{rot}Q_{vib}$, were calculated from B3LYP/6-31+G-(2d,p) frequencies and moments of inertia. These thermal rate constants were fitted into Arrhenius equations to yield the activation parameters, log A and E_{arrh}. The dissociation showed a linear Arrhenius plot of log k_{dis} versus $1/T$, $r^2 = 0.99998$, with log $A = 14.14$ and $E_{arrh} = 63.8$ kJ mol^{-1}. The calculated rate constant was $k_{dis} = 1064$ s^{-1} at 300 K. This implied that at the high-pressure limit **1** should have a lifetime of 0.65 ms at room temperature and thus must represent a short-lived transient intermediate. The Arrhenius plot of log k_{add} versus $1/T$ for the addition reaction showed a slight curvature in the 200−350 K temperature interval (Figure 9). Linear fit in a narrow interval of 270−300 K gave log $A = 12.19$ and $E_{arrh} = 5.4$ kJ mol^{-1}, $r^2 = 0.9996$. A tighter fit over the entire temperature range was obtained by using an empirical formula, $k = A \times T^n \times e^{-E_a/RT}$, where $A = 10^{3.8024}$, $n = 2.9035$, and $E_a = -1.4228$ kJ mol^{-1}. The $k_{295} = 1.68 \times 10^{11}$ cm^3 mol^{-1} s^{-1} calculated from eq 12 was in excellent agreement with the experimental value of Simons and co-workers,[71] $k_{295} = 1.75 \pm 0.25 \times 10^{11}$ cm^3 mol^{-1} s^{-1}. The calculated $k_{298} = 1.72 \times 10^{11}$ cm^3 mol^{-1} s^{-1} was somewhat higher than the older experimental value of $k_{298} \approx 7.6 \times 10^{10}$ reported by Calvert et al.[72]

Franck−Condon Energies. The energy content of radicals formed by collisional neutralization is often governed by Franck−Condon (FC) effects in the fast electron transfer.[73] The Franck−Condon energies for vertical neutralization, ionization, and the corresponding radical ionization energies and ion recombination energies are summarized in Table 2. The calculated ion recombination energies revealed low (2 kJ mol^{-1}) to moderate (43 kJ mol^{-1}) FC effects in vertical neutralization of $\mathbf{2a}^+$ and $\mathbf{2s}^+$, respectively. Hence, the internal excitation in **2s** and **2a** due to FC effects alone was insufficient to cause radical dissociation. By contrast, vertical neutralization of $\mathbf{1}^+$, $\mathbf{3s}^+$, $\mathbf{3a}^+$, $\mathbf{4}^+$, and $\mathbf{5}^+$ resulted in substantial excitation in the radicals formed (Table 1). In particular, the FC energy deposited in vertically formed **1** (141 kJ mol^{-1}) substantially exceeded the C−S bond dissociation energy (59 kJ mol^{-1}). Hence, fast dissociation of vertically formed **1** could be expected and was observed by experiment. The origin of the large FC effect in **1** was examined by comparing the relaxed geometries of $\mathbf{1}^+$ and **1** (Figures 4 and 6). The optimized bond lengths in $\mathbf{1}^+$ and **1** differed only slightly (Figures 4 and 6) and presumably did not give rise to the large FC energy. A major difference was in the spatial arrangement of the oxygen and carbon atoms about the sulfur atom, which was planar in $\mathbf{1}^+$ and 54° pyramidal in **1**. The potential energy for planarization on sulfur in **1** was therefore studied by locating the transition state (**TS7**) for an umbrella flipping at sulfur. The E(**TS7**) = 240 kJ mol^{-1} was unusually large and exceeded the FC energy upon vertical neutralization.

Laser Photoexcitation of [C, H_3, S, O_2]. The neutralized and reionized beam was irradiated with the main lines, 488 and 514.5 nm, from the argon−ion laser. Typically, two sets of alternating laser-on and laser-off experiments were performed. The laser-on and laser-off experiments were normalized to produce the same total ion current, and the difference spectra in the normalized laser-on and laser-off spectra were obtained. The drift between experiments was estimated by comparing the normalized difference spectra for the first and second laser-on experiments and also for the first and second laser-off experiments.

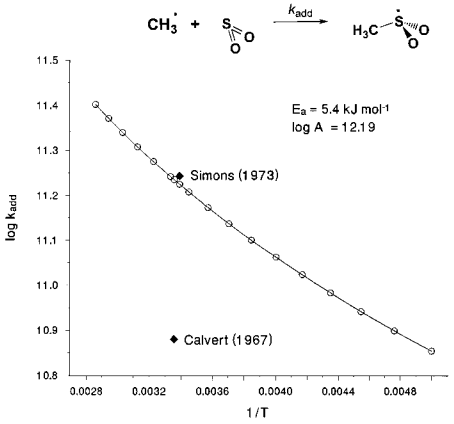

Figure 9. Calculated Arrhenius plot for CH_3 addition to the sulfur atom in SO_2.

TABLE 2: G2(PMP2) Ionization, Recombination, and Franck−Condon Energies

species	IE_a(eV)[a]	IE_v(eV)[b]	RE_v(eV)[c]	E_{FC}(kJ mol^{-1})
1	8.64	9.62		95
2a	8.19	8.67		45
2s	8.09	8.72		60
3s	7.14			
3a	7.08			
4	8.31			
5	7.72			
$\mathbf{1}^+$			7.17	141
$\mathbf{2a}^+$			7.74	44
$\mathbf{2s}^+$			8.07	2
$\mathbf{3a}^+$			5.45	163
$\mathbf{3s}^+$			5.27	174
$\mathbf{4}^+$			6.67	158
$\mathbf{5}^+$			5.65	200

[a] Adiabatic ionization energy. [b] Vertical ionization energy. [c] Vertical recombination energy.

In general, the changes in the NR and photoexcitation NR spectra were small (up to 10% relative) for either **2s,a** or **1**. However, the normalized difference spectra indicated consistent changes for the survivor ion of **2s,a** and the $SO^{+\bullet}$ fragment. In the presence of the laser radiation, the survivor ion of **2s,a** was observed to increase slightly regardless of the variations in the relative abundances observed for several subsequently measured spectra. The $SO^{+\bullet}$ peak decreased slightly during irradiation. The laser-induced decrease in [$SO^{+\bullet}$] was about twice the relative intensity drift in the same direction and was assigned to photoexcitation. The photoexcitation experiments for the **1** and $\mathbf{1}^+$ did not indicate significant changes in the NR difference spectra which could be attributed to photoexcitation. In addition, the photoexcitation experiments on SO_2 did not indicate changes in the NR spectrum which would exceed relative intensity variations.

In a second series of photoexcitation experiments, a solid optical stop was installed on the chicane energy filter lens. This allowed irradiation of the reionized ion beam while prohibiting irradiation of the neutral beam. Therefore, ionic dissociations due to photoexcitation events could be elucidated and compared to the neutral/ion beam irradiation experiments. The photoexcitation of reionized $\mathbf{2s,a}^+$ indicated very small decreases in

TABLE 3: Excitation Energies and Oscillator Strengths of Electronic States in 1 and 2s

	1		2	
state	ΔE(eV)[a]	f[b]	ΔE(eV)[a]	f[b]
X	0		0	
X(VN)[c]	1.14		0.04	
A	3.62	0.034	4.02	0.0026
A(VN)[c]	3.31	0.0057	5.05	0.0006
A(opt)[d]	–		2.26	0.0000
B	4.20	0.0046	4.87	0.047
B(VN)[c]	7.20	0.0001	5.48	0.014
B(opt)[d]	–		4.05	0.049
C	4.41	0.011	5.21	0.0012
C(VN)[c]	7.62	0.042	5.53	0.010
D	6.79	0.043	6.00	0.0024
D (VN)[c]	7.72	0.0041	6.26	0.044
E	7.39	0.047	6.26	0.0052
E(VN)[c]	7.82	0.0036	6.61	0.017

[a] CIS/6-311+G(3df,2p) energies relative to the energy of the geometry-optimized *X* state. [b] Oscillator strengths for transitions to the *X* state of the same geometry. [c] Single-point calculations on optimized ion geometries corresponding to vertical electron capture. [d] Optimized excited-state geometries.

the [SOH^+], [CH_2OH^+], and [$O^{+\bullet}$] which were opposite the drift in the spectra. However, no other changes were observed to occur for photoexcitation events due to the reionized ionic beam only. Photoexcitation of $SO_2^{+\bullet}$ was performed and did not indicate significant changes in the NR spectra. The ability of $SO^{+\bullet}$ to absorb under the current experimental conditions was examined and indicated that a small decrease occurred in the survivor ion upon photoexcitation that was in addition to the drift.

Excited Electronic States of 1 and 2s. Regarding the photoexcitation experiments, we examined with CIS calculations the five lowest excited states in **1** and **2s**. This was done for geometries corresponding to vertical electron capture in ions $\mathbf{1}^+$ and $\mathbf{2s}^+$, for optimized radical geometries corresponding to vertical excitation of relaxed ground states of **1** and **2s**, and for relaxed, fully optimized geometries of the excited states in **2s**. The relative energies from single-point CIS/6-311+G(3df,2p) calculations are summarized in Table 3. The excited states produced by promoting the 21α (SOMO) electron to the virtual α-orbital space are denoted as α-states; those due to promotion of inner β-electrons to 21β (SOMO) and virtual β-orbital space are denoted as β-states; and those due to mixed α and β-electron excitations are denoted as αβ-states. The ordering of excited states in **1** and **2s** is shown in Figures 10 and 11.

The first excited state (*A*) of **1** calculated for the ion geometry was an α-state. The CIS wave function for the *A* state had a substantial ($c_i = 0.723$) but not dominant contribution from the determinant due to a 21α → 22α excitation. The *A* state was 3.31 eV above the relaxed ground (*X*) state of **1** and 2.17 eV above the point of vertical landing on the *X* state potential energy surface. The FC energy for the *X* state was 110 kJ mol^{-1} at the UHF/6-311+G(3df,2p) level of theory. The higher excited states had substantially greater excitation energies; e.g., *B*(α), *C*(β), *D*(α), and *E*(α) (Table 3). Note that the α-states (*A*, *B*, *D*, and *E*) can be produced by direct vertical electron capture in $\mathbf{1}^+$, whereas formation of the β-states would require more substantial reorganization, including paired valence electrons.

The ordering of the excited states was different for vertical excitation of the vibrationally relaxed *X* state of **1** (Table 3). These calculations were performed with C_s molecular geometry for **1**. The four lowest excited states, (^{2}A″)*A*, (^{2}A″)*B*, (^{2}A′)*C*, and (^{2}A′)*D*, were β-states with large contributions of determinants resulting from 20β → 21β ($c_i = 0.884$), 18β → 21β ($c_i = 0.880$), 19β → 21β ($c_i = 0.901$), and 17β → 21β ($c_i = 0.821$) excitations, respectively. The fifth state, (^{2}A′)*E*, was an α-state.

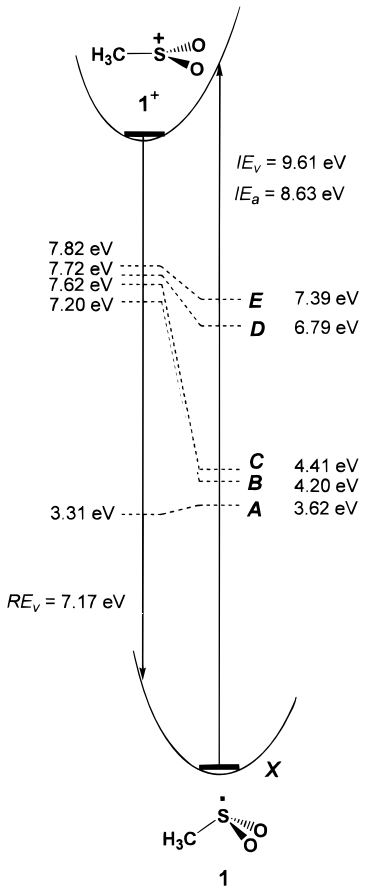

Figure 10. Potential energy diagrams of excited states in **1**.

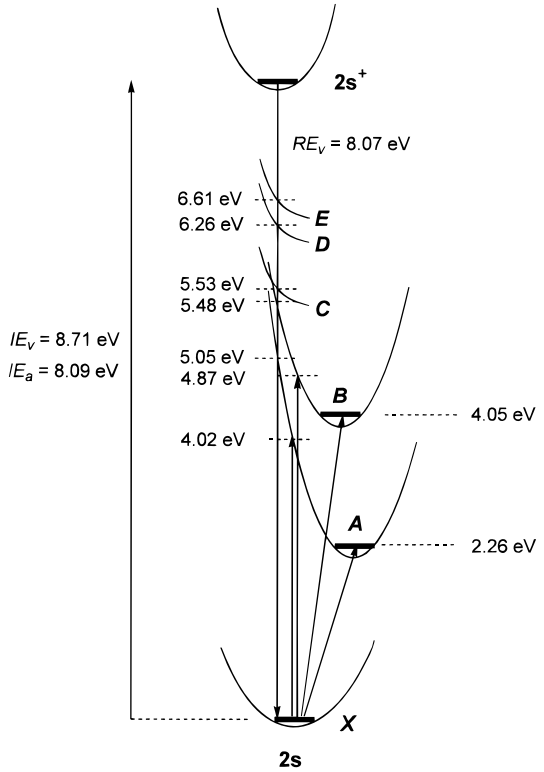

Figure 11. Potential energy diagrams of excited states in **2s**.

Optimization of the *A* state starting from the ion geometry maintained the near-planar geometry about the sulfur atom. However, the optimization was impaired by mixing of the α and *β* states, which resulted in intermediate geometries that oscillated and did not lead to a final local minimum. It should be noted that previous MP2 calculations of McKee provided a pyramidal ^{2}A" excited state for **1**.[8]

The excited states of **2s** calculated for the ion geometry were mostly mixed states, *A*(α*β*), *B*(α*β*), *C*(α*β*), *D*(*β*), and *E*(α), which were ≥ 5 eV above the *X* state (Table 3). Note that the FC energy of the vertically formed *X* state was low, 2−4 kJ mol^{-1} at all levels of theory (Table 3). Vertical excitation in the vibrationally relaxed *X* state of **2s** gave low lying *β*-states (*A* and *B*), α-states (*C* and *D*), and a mixed α*β*-state (*E*). Geometry optimization of the *A*(*β*) state resulted in a structure with an elongated terminal S−O bond and the methyl group rotated perpendicular to the O−S−O plane (Figure 6). The optimized *A*(*β*) state was 2.26 eV above the relaxed *X* state and had a negligible oscillator strength (<0.0001) for radiative transition to the *X* state. The *B* state was also fully optimized to give a geometry which resembled that of the *X* state (Figure 6). The CIS wave function of the *B* state had a dominant contribution (0.910) from the determinant due to 20*β* → 21*β* excitation. The *B* state energy was 4.05 eV above the relaxed *X* state of **2s**. Comparison of the energies for the optimized geometries and those formed by vertical neutralization revealed large FC effects, e.g., 270 and 138 kJ mol^{-1} for the *A* and *B* states, respectively.

Attempted optimizations of the *C*, *D*, and *E* states led to dissociation of the terminal O−S bond to form CH_3OS and an O atom. The dissociations converged to a single electronic state that included a dominant contribution from a 21α → 22α electron excitation. In connection with this dissociation, the 0 K threshold energy for the formation of $CH_3OS^{\bullet}$ and (^{3}P)O was calculated by G2(MP2) as 483 kJ mol^{-1} relative to (*X*) **2s**. Hence, if formed vertically in the *C* through *E* states, **2s** should have a sufficient internal energy to dissociate to CH_3OS and (^{3}P)O.

Discussion

The experimental data and ab initio calculations are now discussed to provide a comprehensive picture of the formation and dissociations of ions $\mathbf{1}^+$ and $\mathbf{2}^+$ and radicals **1** and **2**. Ions $\mathbf{2s}^+$ and $\mathbf{2a}^+$ are the most stable $[C, H_3, S, O_2]^+$ isomers, and their formation by simple bond cleavage in ionized dimethyl sulfite (Scheme 1) should be straightforward. In contrast, the formation of the less stable isomer $\mathbf{1}^+$ by dissociation of ionized methyl sulfone may depend on the reaction energetics. The photoelectron spectrum of methyl sulfone[74] shows a band at IE_4 = 12.00 eV, which corresponds to a dissociative state of $(CH_3)_2SO_2^{+\bullet}$ decomposing to $CH_3^{\bullet}$ and $\mathbf{1}^+$ of 11.91 eV threshold energy (vide supra). The next available electronic states in $(CH_3)_2SO_2^{+\bullet}$ are at 14.52 and 16.37 eV.[74] Dissociations to $CH_3^{\bullet}$ + $\mathbf{1}^+$ from these higher states are 252 and 430 kJ mol^{-1} exothermic. If this energy were deposited in $\mathbf{1}^+$, it would cause its rapid dissociation (Figure 5). However, if a 136−164 kJ mol^{-1} fraction of the available dissociation exothermicity was deposited in $\mathbf{1}^+$, it would cause equilibration with $\mathbf{2}^+$, which would greatly prefer the latter. It is therefore possible that $\mathbf{1}^+$ formed by dissociative ionization of methyl sulfone could be contaminated with a small fraction of $\mathbf{2s,a}^+$. In contrast, $\mathbf{1}^+$ formed by charge-exchange ionization with Xe^+ should be pure for the same energy reasons.

The NR mass spectrum of $\mathbf{1}^+$ produced by electron impact ionization of methyl sulfone showed a small fraction of survivor ions resulting from nondissociating radicals. In contrast, $\mathbf{1}^+$ produced by charge-exchange ionization with Xe did not give survivor radicals and ions upon NRMS. The radical dissociations and the nature of the surviving radicals from $\mathbf{1}^+$, therefore, need to be discussed. According to the calculations, vertical neutralization of vibrationally relaxed (all $n = 0$) $\mathbf{1}^+$ resulted in a vibrationally highly excited **1** due to the large Franck−Condon energy (141 kJ mol^{-1}). The RRKM dissociation kinetics indicated that, at this excitation, the unimolecular rate constant should be >10^{12} s^{-1}, implying subpicosecond lifetimes for **1** (Figure 8). The variable-time measurements cannot resolve such fast dissociations.[44] However, a fraction of **1** undergoing very fast dissociations can be incorporated into the kinetic equations as a parameter.[44a] The kinetic data for **1** showed the best fit by convoluting 90% of fast dissociations with 10% of those occurring on the microsecond time scale, k_N, vide supra. The occurrence of fast dissociations of vertically formed **1** was therefore consistent with the kinetic data.

The substantial energy barriers to dissociations of **2s,a** (vide supra) were in accord with the observation of >14% nondissociating radicals. The RRKM calculations indicated that direct C−O bond cleavage in **2s,a** was considerably slower than isomerization to hot **1**, which, when thus formed, must dissociate rapidly (k > 10^{11} s^{-1}) to $CH_3^{\bullet}$ and SO_2 (Figure 8). The energy driving the unimolecular dissociation of **2s,a** could not be supplied fully by FC effects on vertical neutralization, because the corresponding FC energies were small to moderate (vide supra). The fraction of dissociating radicals **2s,a** thus must have received a major part of the vibrational energy from the precursor ions. This also provided a clue for the question of $\mathbf{2s,a}^+$ contaminating $\mathbf{1}^+$. A fraction of $\mathbf{2s,a}^+$ formed by unimolecular isomerization of $\mathbf{1}^+$ must have >190 kJ mol^{-1} internal energy after overcoming the ion isomerization barrier. If combined with the FC energy on neutralization, the radicals **2s,a** formed will have >200 kJ mol^{-1} internal energy. However, RRKM calculations indicated that at this excitation **2s,a** would isomerize back to **1** and dissociate with k > 10^9 s^{-1} (Figure 8). Hence, high-energy but nondissociating $\mathbf{2s,a}^+$ at equilibrium with $\mathbf{1}^+$ could not give rise to radicals of microsecond lifetimes which were observed in the NR mass spectrum of $\mathbf{1}^+$.

A plausible explanation of the latter phenomenon is based on an analysis of the FC effects.[73b,c] While the geometry of vibrationally relaxed $\mathbf{1}^+$ showed a large mismatch with that of relaxed **1**, the mismatch could be alleviated by vertical transition between an *excited vibrational state* of $\mathbf{1}^+$ of nonrelaxed geometry and a lower vibrational state of **1**. In particular, the out-of-plane deformation vibration in $\mathbf{1}^+$ at $\nu = 336$ cm^{-1} was expected to be excited to n > 0 states in hot $\mathbf{1}^+$. For $\mathbf{1}^+$ of internal energies limited above by the isomerization barrier to $\mathbf{2a}^+$ (135 kJ mol^{-1}), the distribution of vibrational states, $P_j(n)$, for the $\nu_j = 336$ cm^{-1} mode was obtained from Dunbar's equilibrium formula for a harmonic oscillator (eq 13),[75] where *h*, *c*, and *k* are the Planck constant, speed of light,

$$P_j(n) = e^{-nhc\nu_j/kT} \times \{e^{-(k/2C_v)(nhc\nu_j/kT)^2} - e^{-hc\nu_j/kT} \times e^{-(k/2C_v)((n+1)hc\nu_j/kT)^2}\} \quad (13)$$

and Boltzmann constant, respectively. The effective temperature was approximated as $T = H_{vib,T}/C_{vib,T} = 1770$ K, where $H_{vib,T}$ = 135 kJ mol^{-1} was the limit for the vibrational energy of stable $\mathbf{1}^+$ and $C_{vib,T}$ was the pertinent vibrational heat capacity. The calculated distribution showed 76% of the $\nu = 336$ cm^{-1} mode in $n > 1$ states, whereby states up to $n = 11$ were populated >1%. Neutralization of these high vibrational states of the

deformation mode was expected to produce **1** with a nonplanar geometry, which should reduce the FC energy close to or below the 59 kJ mol^{-1} dissociation limit. Similar effects have been observed previously for silicon-centered radicals.[73c] Note finally that the RRKM curve for dissociation of **1** showed a rapid increase of k_{dis} with internal energy. Hence, stabilization by a kinetic shift[76] should be negligible in **1**.

The photoexcitation experiments revealed depletion of $SO^{+\bullet}$ and an increased fraction of survivor $\mathbf{2s}^+$ and/or $\mathbf{2a}^+$ following irradiation of the neutral and reionized ion beam. The first effect was also observed for the reionized beam of $SO^{+\bullet}$ alone and can be ascribed unambiguously to ion photofragmentation. A previous study by Cosby showed that irradiation of $SO^{+\bullet}$ with 575−690 nm photons caused photodissociation which was assigned to excitation from high vibrational states of the ground electronic state of the ion.[77]

The increased fraction of survivor $\mathbf{2s}^+$ and/or $\mathbf{2a}^+$ was not due to photoexcitation of the cations, which did not absorb at the wavelengths used. Hence, the effect must be due to interaction with the 488 and 514.5 nm photons of the intermediate radicals, **2s** and/or **2a**. The calculated CIS energies (Table 3) indicated that the (*X*) state of **2s** should not absorb at the wavelengths used. This was predicted for both vertically formed **2s**, where the energy gap $X \rightarrow A$ was 5.05 eV, and relaxed *X* and *A* states, where the transition was dipole-forbidden. The optimized geometry of the *A* state of **2s** was very different from the geometry of both $\mathbf{2s}^+$ and the *X* state of **2s**, as illustrated by the large FC energies accompanying electron capture, $\mathbf{2s}^+ \rightarrow$ (*A*)**2s**, and $X \rightarrow A$ excitation (Table 3). It is therefore unlikely that the *A* state of **2s** was significantly populated by vertical neutralization of the ion. The *B* state of **2s** was bound and its radiative lifetime increased when the radical was formed with the ion geometry (Table 3). The *C*, *D*, and *E* states were dissociative.

The increased fraction of $\mathbf{2s,a}^+$ may be due to an increased fraction of *nondissociating* **2s**,**a**. This fraction can be formed by stimulated photon emission from a bound state, such as *B*, to the stable *X* state. It should be noted, however, that such a process would be nonresonant and therefore of low efficiency. Alternatively, photoexcitation of **2s** formed in the *B* state could lead to the population of a higher excited state. The energy data indicate that a vertically formed *B* state of 5.48 eV energy absorbing a 2.54 eV photon could produce a *high Rydberg state* of **2s** ($\Delta E = 8.02$ eV), which is still below the adiabatic (8.09 eV) and vertical (8.71 eV) ionization limits of **2s**. Excitation to a Rydberg state could substantially increase the cross section for collisional ionization of **2s**. Collisional cross sections of radicals have been estimated to scale with n^4, where *n* is the principal quantum number of the Rydberg state.[45c] The steep increase of the ionization cross section could explain the increased intensity of $\mathbf{2s}^+$ and/or $\mathbf{2a}^+$ observed upon irradiation even if the population of the *B* state and the photoexcited fractions were small.

Finally, it may be noted that the properties of the [C, H_3, S, O_2] ions and radicals paralleled those of the homologous [S, O_2, H] species.[40b] In particular, when formed by vertical neutralization of the corresponding cations, both **2s,a** and HO−S−O$^\bullet$ radicals underwent highly endothermic S−O bond cleavages with microsecond kinetics, which were interpreted as occurring on excited-state potential energy surfaces. It appears that the formation of metastable excited electronic states upon vertical electron transfer is a common phenomenon[40,45] that has often been overlooked in the previous NRMS studies.

Conclusions

The methylsulfonyl (**1**) and methoxysulfinyl (**2**) radicals are predicted to be stable species in the gas phase. When formed by vertical collisional electron transfer from cation $\mathbf{1}^+$, radical **1** dissociates to $CH_3^\bullet$ and SO_2 because of a large Franck−Condon energy associated with the neutralization. A small fraction of nondissociating **1** is observed on neutralization of hot cations $\mathbf{1}^+$ in which vibrational excitation of the out-of-plane deformation mode results in an improved match between the ion and incipient radical geometries and thus diminishes the Franck−Condon energy in vertical electron transfer. Radical **2** exists as a mixture of syn (**2s**) and anti (**2a**) isomers, which are stable when formed by collisional electron transfer to the corresponding cations. The lowest-energy dissociation of **2s** and **2a** forms $CH_3^\bullet$ and SO_2 via isomerization to **1**. Collisional neutralization of $\mathbf{2s,a}^+$ produced a fraction of an excited *B* state of **2s,a**, which was probed by laser photoexcitation. It is concluded that photoexcitation of the *B* state produced a high Rydberg state of a large collisional cross section, which was efficiently ionized by collisions with oxygen.

Acknowledgment. Support of this work by the National Science Foundation (Grant CHE-9712570) is gratefully acknowledged. We thank Martin Sadilek and Miroslav Polasek for technical assistance.

Supporting Information Available: Tables of B3LYP/6-31+G(2d,p) and UMP2(FULL)/6-31+G(2d,p) geometries, B3LYP/6-31+G(2d,p) harmonic frequencies, and G2(MP2) total energies. This information is available free of charge via the Internet at http://pubs.acs.org.

References and Notes

(1) Wayne, R. P. *Chemistry of Atmospheres*; Oxford: New York, 1993; Chapter 1.
(2) Cullis, C. F.; Hirschler, M. M. *Atmospheric Environment* **1980**, *14*, 1263.
(3) Tyndall, G. S.; Ravishankara, A. R. *Int. J. Chem. Kinet.* **1991**, *23*, 483.
(4) Charlson, R. J.; Lovelock, J. E. *Nature* **1987**, *326*, 655.
(5) Trindle, C.; Romberg, K. *J. Phys. Chem. A* **1998**, *102*, 270−273.
(6) Laakso, D.; Smith, C. E.; Goumri, A.; Rocha, J.-D. R.; Marshall, P. *Chem. Phys. Lett.* **1994**, *227*, 377.
(7) Davis, S. R. *J. Phys. Chem.* **1993**, *97*, 7535.
(8) McKee, M. L. *Chem. Phys. Lett.* **1993**, *211*, 643.
(9) Boyd, R. J.; Gupta, A.; Langler, R. F.; Lownie, S. P.; Pincock, J. A. *Can. J. Chem.* **1980**, *58*, 331.
(10) Gozdz, A. S. *Macromolecules* **1990**, *23*, 910.
(11) Culshaw, P. N.; Walton, J. C. *Tetrahedron Lett.* **1990**, *31*, 2457.
(12) Swarts, S. G.; Becker, D.; DeBolt, S.; Sevilla, M. D. *J. Phys. Chem.* **1989**, *93*, 155.
(13) Bennett, J. E.; Brunton, G.; Silbert, B. C.; Whittall, P. E. *J. Chem. Soc., Perkin Trans. 2* **1988**, 1359.
(14) Chatgilialoglu, C.; Griller, D.; Guerra, M. *J. Phys. Chem.* **1987**, *91*, 3747.
(15) Chatgilialoglu, C.; Gilbert, B. C.; Norman, R. O. C. *J. Chem. Soc., Perkin Trans. 2* **1980**, *10*, 1429.
(16) Gilbert, B. C.; Kirk, C. M.; Norman, R. O. C. *J. Chem. Res., Synop.* **1977**, 173.
(17) Andersen, R. S. *J. Chem. Phys.* **1977**, *66*, 5610.
(18) Eriksen, T. E.; Lind, J. *Radiochem. Radioanal. Lett.* **1976**, *25*, 11.
(19) Eriksen, T. E.; Lind, J.; Gillbro, T. *Int. J. Radiat. Phys.* **1976**, *8*, 655.
(20) Gilbert, B. C.; Norman, R. O. C.; Sealy, R. C. *J. Chem. Soc., Perkin Trans. 2* **1975**, *3*, 1975.
(21) Flockhart, B. D.; Ivin, K. J.; Pink, R. C.; Sharma, B. D. *J. Chem. Soc. D* **1971**, *7*, 339.
(22) Good, A.; Thynne, J. C. *J. Chem. Soc., Faraday Trans. 1* **1967**, *63*, 2708.
(23) James, F. C.; Kerr, J. A.; Simons, J. P. *J. Chem. Soc., Faraday Trans. 1* **1973**, *63*, 2124.
(24) Turnipseed, A. A.; Barone, S. B.; Ravishankara, A. R. *J. Phys. Chem.* **1993**, *97*, 5926.

(25) Domine, F.; Ravishankara, A. R.; Howard, C. J. *J. Phys. Chem.* **1992**, *96*, 2171.
(26) Turnipseed, A. A.; Barone, S. B.; Ravishankara, A. R. *J. Phys. Chem.* **1992,** *96*, 7502.
(27) Domine, F.; Murrells, T. P.; Howard, C. J. *J. Phys. Chem.* **1990**, *94*, 5839.
(28) Tyndall, G. S.; Ravishankara, A. R. *J. Phys. Chem.* **1989**, *93*, 2426.
(29) Moraes, L. A. B.; Eberlin, M. N. *J. Chem. Soc., Perkin Trans. 2* **1997**, 2105.
(30) Gozzo, F. C.; Sorrilha, A. E. P. M.; Eberlin, M. N. *J. Chem. Soc., Perkin Trans. 2* **1996**, 587.
(31) de Petris, G.; Fornarini, S.; Occhiucci, G. *Int. J. Mass Spectrosc. Ion Proc.* **1992**, *112*, 231.
(32) Chatgilialoglu, C.; Guerra, M.; Pelli, B.; Traldi, P. *Org. Mass Spectrosc.* **1989**, *24*, 455.
(33) For reviews see: (a) Wesdemiotis, C.; McLafferty, F. W. *Chem. Rev.* **1987**, *87*, 485. (b) Terlouw, J. K.; Schwarz, H. *Angew. Chem., Int. Ed. Engl.* **1987**, *26*, 805. (c) Holmes, J. L. *Mass Spectrom. Rev.* **1989**, *8*, 513. (d) Terlouw, J. K. *Adv. Mass Spectrom.* **1989**, *11*, 984. (e) McLafferty, F. W. *Science*, **1990**, *247*, 925. (f) Turecek, F. *Org. Mass Spectrom.* **1992**, *27*, 1087. (g) Goldberg, N.; Schwarz, H. *Acc. Chem. Res.* **1994**, *27*, 347. (h) Schalley, C. A.; Hornung, G.; Schroder, D.; Schwarz, H. *Chem. Soc. Rev.* **1998**, *27*, 91.
(34) Iraqi, M.; Goldberg, N.; Schwarz, H. *J. Phys. Chem.* **1994**, *98*, 2015−2017.
(35) Turecek, F.; Drinkwater, D. E.; McLafferty, F. W. *J. Am. Chem. Soc.* **1989**, *111*, 7696−7701.
(36) Egsgaard, H.; Carlsen, L.; Florencio, H.; Drewello, T.; Schwarz, H. *Chem. Phys. Lett.* **1988**, *148*, 537−540.
(37) Sulzle, D.; Verhoeven, M.; Terlouw, J. K.; Schwarz, H. *Angew. Chem., Int.* **1988**, *100*, 1591−1592.
(38) Turecek, F.; McLafferty, F. W.; Smith, B. J.; Radom, L. *Int. J. Mass Spectrom. Ion Processes* **1990**, *101*, 283−300.
(39) Gu, M.; Turecek, F. *J. Am. Chem. Soc.* **1992**, *114*, 7146−7151.
(40) (a) Frank, A. J.; Sadilek, M.; Ferrier, J. G.; Turecek, F. *J. Am. Chem. Soc.* **1996**, *118*, 11321−11322. (b) Frank, A. J.; Sadilek, M.; Ferrier, J. G.; Turecek, F. *J. Am. Chem. Soc.* **1997**, *119*, 12343−12353.
(41) Schmidt, H.; Steudel, R.; Sulzle, D.; Schwarz, H. *Inorg. Chem.* **1992**, *31*, 941.
(42) Iraqi, M.; Schwarz, H. *Chem. Phys. Lett.* **1994**, *221*, 359.
(43) Flammang, R.; Wentrup, C. *Sulfur Rep.* **1997**, *20*, 255−278.
(44) (a) Kuhns, D. W.; Tran, T. B.; Shaffer, S. A.; Turecek, F. *J. Phys. Chem.* **1994**, *98*, 4845−4853. (b) Kuhns, D. W.; Turecek, F. *Org. Mass Spectrom.* **1994**, *29*, 463−469. (c) Sadilek, M.; Turecek, F. *J. Phys. Chem.* **1996**, *100*, 224−232.
(45) (a) Sadilek, M.; Turecek, F. *J. Phys. Chem.* **1996**, *100*, 9610−9614. (b) Sadilek, M.; Turecek, F. *Chem. Phys. Lett.* **1996**, *263*, 203−208. (c) Nguyen, V. Q.; Sadilek, M.; Frank, A. J.; Ferrier, J. G.; Turecek, F. *J. Phys. Chem. A* **1997**, *101*, 3789−3799.
(46) (a) Gilbert, R. G.; Smith, S. C. *Theory of Unimolecular and Recombination Reactions*; Blackwell: London, 1990. (b) Baer, T.; Hase, W. L. *Unimolecular Reaction Dynamics. Theory and Experiment*; Oxford: New York, 1996. (c) Hase, W. L. *Acc. Chem. Res.* **1998**, *31*, 659−665.
(47) Turecek, F.; Gu, M.; Shaffer, S. A. *J. Am. Soc. Mass Spectrom.* **1992**, *3*, 493.
(48) Fitch, W. L.; Sauter, A. D. *Anal. Chem.* **1983**, *55*, 832.
(49) Frisch, M. J.; Trucks, G. W.; Schlegel, H. B.; Gill, P. M. W.; Johnson, B. G.; Robb, M. A.; Cheeseman, J. R.; Keith, T. A.; Petersson, G. A.; Montgomery, J. A.; Raghavachari, K.; Al-Laham, M. A.; Zakrzewski, V. G.; Ortiz, J. V.; Foresman, J. B.; Cioslowski, J.; Stefanov, B. B.; Nanayakkara, A.; Challacombe, M.; Peng, C. Y.; Ayala, P. Y.; Chen, W.; Wong, M. W.; Andres, J. L.; Replogle, E. S.; Gomperts, R.; Martin, R. L.; Fox, D. J.; Binkley, J. S.; Defrees, D. J.; Baker, J.; Stewart, J. P.; Head-Gordon, M.; Gonzalez, C.; Pople, J. A. *Gaussian 94*; Gaussian, Inc.: Pittsburgh, PA, 1995.
(50) (a) Becke, A. D. *J. Chem. Phys.* **1993**, *98*, 1372, 5648. (b) Stephens, P. J.; Devlin, F. J.; Chablowski, C. F.; Frisch, M. J. *J. Phys. Chem.* **1994**, *98*, 11623.
(51) Hehre, W. J.; Radom, L.; Pople, J. A. *Ab Initio Molecular Orbital Theory*; Wiley: New York, 1986; pp 82−88.
(52) See for example: (a) Bauschlicher, C. W.; Partridge, H. *J. Chem. Phys.* **1995**, *103*, 1788. (b) Turecek, F. *J. Phys. Chem. A*, **1998**, *102*, 4703−4713.
(53) (a) Xantheas, S. S.; Dunning, T. H., Jr. *J. Phys. Chem.* **1993**, *97*, 6616. (b) McKee, M. L. *J. Phys. Chem.* **1993**, *97*, 10971−10976. (c) Smart, B. A.; Schiesser, C. H. *J. Comput. Chem.* **1995**, *16*, 1055. (d) Ruttink, P. J. A.; Burgers, P. C.; Francis, J. T.; Terlouw, J. K. *J. Phys. Chem.* **1996**, *100*, 9694.
(54) Møller, C.; Plesset, M. S. *Phys. Rev.* **1934**, *46*, 618.
(55) Schlegel, H. B. *J. Chem. Phys.* **1986**, *84*, 4530−4534.
(56) (a) Rauhut, G.; Pulay, R. *J. Phys. Chem.* **1995**, *99*, 3093. (b) Finley, J. W.; Stephens, P. J. *J. Mol. Struct. (THEOCHEM)* **1995**, *357*, 225. (c) Wong, M. W. *Chem. Phys. Lett.* **1996**, *256*, 391. For different scaling factors see: (d) Scott, A. P.; Radom, L. *J. Phys. Chem.* **1996**, *100*, 16502.
(57) (a) Curtiss, L. A.; Raghavachari, K.; Pople, J. A. *J. Chem. Phys.* **1993**, *98*, 1293. (b) Curtiss, L. A.; Raghavachari, K.; Redfern, P. C.; Pople, J. A. *J. Chem. Phys.* **1997**, *106*, 1063. (c) Raghavachari, K.; Stefanov, B. B.; Curtiss, L. A. *J. Chem. Phys.* **1997**, *106*, 6764.
(58) Pople, J. A.; Head-Gordon, M.; Raghavachari, K. *J. Chem. Phys.* **1987**, *87*, 5968.
(59) Foresman, J. B.; Head-Gordon, M.; Pople, J. A.; Frisch, M. J. *J. Phys. Chem.* **1992**, *96*, 135−149.
(60) Zhu, L.; Hase, W. L. *Quantum Chemistry Program Exchange*; Indiana University: Bloomington, IN, 1994; Program No. QCPE 644.
(61) Zhu, L.; Hase, W. L. *Chem. Phys. Lett.* **1990**, *175*, 117−123.
(62) (a) Munson, M. S. B.; Franklin, J. L. *J. Phys. Chem.* **1964**, *6*, 8, 3191. (b) Bowen, R. D.; Williams, D. H. *J. Chem. Soc., Chem. Commun.* **1977**, 378. (c) Schleyer, P. v. R.; Jemmis, A. D.; Pople, J. A. *J. Chem. Soc., Chem. Commun.* **1978**, 190. (d) Bursey, M. M.; Hass, J. R.; Harvan, D. J.; Parker, C. E. *J. Am. Chem. Soc.* **1979**, *101*, 5485. (e) Burgers, P. C.; Holmes, J. L. *Org. Mass Spectrom.* **1984**, *19*, 452. (f) Yarkony, D. R.; *J. Am. Chem. Soc.* **1992**, *114*, 5406. (g) Kuo, S.-C.; Zhang, Z.; Klemm, R. B.; Liebman, J. F.; Stief, L. I.; Nesbitt, F. L. *J. Phys. Chem.* **1994**, *98*, 4026. (h) Aschi, M.; Harvey, J. N.; Schalley, C. A.; Schroder, D.; Schwarz, H. *J. Chem. Soc., Chem. Commun.* **1998**, 531.
(63) (a) Carpenter, B. K. *J. Am. Chem. Soc.* **1983**, *105*, 1700−1701. (b) Dewar, M. J. S.; Merz, K. M., Jr. *J. Am. Chem. Soc.* **1986**, *108*, 5634−5635.
(64) Mallard, W. G.; Linstrom, P. J., Eds. *NIST Chemistry Webbook*, NIST Standard Reference Database, No. 69, March 1998. National Institute of Standards and Technology: Gaithersburg, MD. http//webbook.nist.gov/chemistry.
(65) The error limits are one standard deviation of the calculated $\Delta H_{f,298}$ and do not include uncertainties in the experimental standard heats of formation.
(66) Kimura, K.; Katsumata, S.; Achiba, Y.; Yamazaki, T.; Iwata, S. *Handbook of He(I) Photoelectron Spectra of Fundamental Organic Molecules*; Japan Scientific Societies Press: Tokyo, 1981; p 23.
(67) (a) Nguyen, M. T.; Creve, S.; Vanquickenborne, L. G. *J. Phys. Chem.* **1996**, *100*, 18422−18425. (b) Turecek, F. *J. Mass Spectrom.* **1998**, *33*, 779−795. (c) McKee, M. L. *J. Am. Chem. Soc.* **1998**, *120*, 3963−3969. (d) Turecek, F.; Wolken, J. K. *J. Phys. Chem. A* **1999**, *103*, 1905.
(68) Amaudrut, J.; Pasto, D. J.; Wiest, O. *J. Org. Chem.* **1998**, *63*, 6061.
(69) Hase, W. L.; Wardlaw, D. M. In *Advances in Gas-Phase Photochemistry and Kinetics*, Ashfold, M. N. R. Baggott, J. E., Eds.; Royal Society of Chemistry: London, 1989; Chapter 4, pp 171−208.
(70) (a) Laidler, K. J.; Polanyi, J. C. In *Progress in Reaction Kinetics*, Porter, G., Ed.; Pergamon: Oxford, 1965; Vol. 3, pp 3−61. (b) Levine, I. N. *Physical Chemistry*, 3rd ed.; McGraw-Hill: New York, 1988; pp. 783−796.
(71) James, F. C.; Kerr, J. A.; Simons, J. P. *J. Chem. Soc., Faraday Trans. 1*, **1973**, 2124−2129.
(72) Sidebottom, H. W.; Badcock, C. C.; Jackson, G. E.; Calvert, J. G.; Reinhardt, G. W.; Damon, E. K. *Environ. Sci. Technol.* **1972**, *6*, 72.
(73) (a) Hop, C. E. C. A.; Holmes, J. L. *Int. J. Mass Spectrom. Ion Processes* **1991**, *104*, 213. (b) Turecek, F.; Gu, M.; Hop, C. E. C. A. *J. Phys. Chem.* **1995**, *99*, 2278−2291. (c) Nguyen, V. Q.; Shaffer, S. A.; Turecek, F.; Hop, C. E. C. A. *J. Phys. Chem.* **1995**, *99*, 15454−15464. (d) Nguyen, V. Q.; Turecek, F. *J. Mass Spectrom.* **1996**, *31*, 843−854.
(74) (a) Muller, C.; Schweig, A. *Tetrahedron* **1973**, *29*, 3973. (b) Solouki, B.; Bock, H.; Appel, R. *Chem. Ber.* **1975**, *108*, 897.
(75) Dunbar, R. C. *J. Chem. Phys.* **1989**, *90*, 7369.
(76) Lifshitz, C. *Mass Spectrom. Rev.* **1982**, *1*, 309.
(77) Cosby, P. C. *J. Chem. Phys.* **1984**, *81*, 1102.